Biophysical Journal
Article

Biophysical Society

Caveolin-3 prevents swelling-induced membrane damage via regulation of $I_{Cl,swell}$ activity

Daniel G. P. Turner,[1] Leonid Tyan,[1] Frank C. DeGuire,[1] Roman Y. Medvedev,[1] Sami J. Stroebel,[1] Di Lang,[1] and Alexey V. Glukhov[1,*]
[1]Department of Medicine, University of Wisconsin-Madison School of Medicine and Public Health, Madison, Wisconsin

ABSTRACT Caveola membrane structures harbor mechanosensitive chloride channels (MCCs; including chloride channel 2, chloride channel 3, and SWELL1, also known as LRRC8A) that form a swelling-activated chloride current ($I_{Cl,swell}$) and play an important role in cell volume regulation and mechanoelectrical signal transduction. However, the role of the muscle-specific caveolar scaffolding protein caveolin-3 (Cav3) in regulation of MCC expression, activity, and contribution to membrane integrity in response to mechanical stress remains unclear. Here we showed that Cav3-transfected (Cav3-positive) HEK293 cells were significantly resistant to extreme (<20 milliosmole) hypotonic swelling compared with native (Cav3-negative) HEK293 cells; the percentage of cells with membrane damage decreased from 45% in Cav3-negative cells to 17% in Cav3-positive cells ($p < 0.05$). This mechanoprotection was significantly reduced ($p < 0.05$) when cells were exposed to the $I_{Cl,swell}$-selective inhibitor 4-[(2-butyl-6,7-dichloro-2-cyclopentyl-2,3-dihydro-1-oxo-1H-inden-5-yl)oxy]butanoic acid (10 μM). These results were recapitulated in isolated mouse ventricular myocytes, where the percentage of cardiomyocytes with membrane damage increased from 47% in control cells to 78% in 4-[(2-butyl-6,7-dichloro-2-cyclopentyl-2,3-dihydro-1-oxo-1H-inden-5-yl)oxy]butanoic acid-treated cells ($p < 0.05$). A higher resistance to hypotonic swelling in Cav3-positive HEK293 cells was accompanied by a significant twofold increase of $I_{Cl,swell}$ current density and SWELL1 protein expression, whereas ClC-2/3 protein levels remained unchanged. Förster resonance energy transfer analysis showed a less than 10-nm membrane and intracellular association between Cav3 and SWELL1. Cav3/SWELL1 membrane Förster resonance energy transfer efficiency was halved in mild (220 milliosmole) hypotonic solution as well as after disruption of caveola structures via cholesterol depletion by 1-h treatment with 10 mM methyl-β-cyclodextrin. A close association between Cav3 and SWELL1 was confirmed by co-immunoprecipitation analysis. Our findings indicate that, in the MCCs tested, SWELL1 abundance and activity are regulated by Cav3 and that their association relies on membrane tension and caveola integrity. This study highlights the mechanoprotective role of Cav3, which is facilitated by complimentary SWELL1 expression and activity.

SIGNIFICANCE Mechanoprotective properties imparted by caveola-generating caveolin-3 (Cav3) expression is facilitated by complimentary SWELL1 mechanosensitive chloride channel expression and activity via a corresponding swelling-activated chloride current ($I_{Cl,swell}$). Cav3-positive HEK293 cells are highly resistant to swelling-induced membrane damage, which is reduced via $I_{Cl,swell}$ inhibition. This effect is also observed in mouse ventricular myocytes. Cav3 expression upregulates the SWELL1 protein expression level and its activity in HEK293 cells. Although all mechanosensitive chloride channels, including chloride channel 2, chloride channel 3, and SWELL-1, associate with the caveolar scaffolding protein Cav3, only the interaction between SWELL1 and Cav3 is dependent on membrane tension and caveola integrity and could be implicated in pathological remodeling of $I_{Cl,swell}$ observed in various cardiac pathologies conditioned by pressure and/or volume overload of the heart that are associated with caveola remodeling.

INTRODUCTION

Several studies have linked various mechanosensitive chloride channels (MCCs) to specialized membrane structures known as caveolae (1–4). These are a subset of lipid rafts that are small (50–100 nm), flask-shaped sarcolemmal membrane invaginations generated by caveolin scaffolding proteins and cavins and are enriched with cholesterol, sphingolipids, and phospholipids (5). Caveolae play an important role in various signal transduction pathways and are known to act as a cell membrane reserve by buffering mechanical forces and contributing to cell volume regulation (6–8). In

Submitted June 18, 2021, and accepted for publication March 31, 2022.
*Correspondence: aglukhov@medicine.wisc.edu
Editor: Michael Grabe.
https://doi.org/10.1016/j.bpj.2022.04.001

the heart, caveolae increase the plasma membrane surface area by 27% in rat ventricular myocytes (9), by 56% in rabbit atrial cells, and by 115% in rabbit sinoatrial node pacemaker cells (10), and cell stretch induced by a hypotonic solution incorporates this reserved membrane into the surface membrane via caveola flattening (6,7). These characteristics allow caveolae to adapt cells to mechanical stress (11,12), facilitate mechanotransduction as mechanosensors (13), and protect cells during pathological events such as ischemia-reperfusion injury (14).

In addition to their ability to influence cell volume, it has been shown in various cell types that caveolae are actively involved in mechanoelectrical feedback, modulating the activation of mechanosensitive ion channels, including MCCs (1,15,16). These interactions are predicted via association of MCCs with the caveolar scaffolding proteins caveolin-1 (Cav1) and caveolin-3 (Cav3) via a complimentary caveolin binding motif (CBM) (17), with Cav3 being a muscle-specific isoform expressed in cardiac, skeletal, and smooth muscle cells (18,19). Caveola-associated localization of MCCs may affect their expression level, trafficking to the membrane, biophysical properties, as well as the response to stretch and various exogenous and endogenous modulators (20–23). MCCs have been found to play a significant role in preventing cell death induced by hypoxia (common in ischemia-reperfusion injury) (24) or hypotonically induced mechanical stress (modeling hypertension) (25). Although our preliminary studies indicate that three MCCs, chloride channel 2 (ClC-2), chloride channel 3 (ClC-3), and SWELL1 (also known as LRRC8A (leucine-rich repeat-containing protein 8 A)), may be associated with Cav3 in rat and human atrial myocardium (1), the mechanisms by which Cav3 prevents cell damage under adverse conditions as well as how Cav3 interacts with these channels and modulates their stretch-related activity remains unknown.

Nearly inactive under resting conditions, MCCs slowly open (>2 min) upon hypotonic swelling and/or cell stretch to regulate cell volume (3). In the heart, MCCs are specifically involved in regulation of cardiac electrical activity and are one of the key components of mechanoelectrical feedback, which is the regulation of cardiac output in response to a change of cardiac pressure and/or volume loading that can alter cardiac action potential morphology (1,26,27). Other channels that can affect this feedback system are activation of mechanoactivated ion currents, including I_{TREK} and I_{TRAAK} (28–30), I_{BK} (31), and I_{NS} (32), and modulation of electrical activity of some of the voltage-gated channels, including I_{CaL} (33), I_{Kur} (32), and I_{K1} (34), which have been linked to various cardiac arrhythmias (26,35,36). Through this mechanoelectrical feedback, MCCs have been linked to stretch-dependent changes in action potential duration and depolarization of the resting membrane potential (1), regulation of sinoatrial node pacemaker automaticity (16,37), arrhythmogenesis (26,36), myocardium hypertrophy (8,38,39), and ischemia-reperfusion damage (38,40). Despite the importance of MCCs in cellular physiology, the molecular identity of the swelling-activated chloride current ($I_{Cl,swell}$) in cardiomyocytes has not been elucidated. Several candidates, including ClC-2, ClC-3, and SWELL1, have been proposed to form $I_{Cl,swell}$ in the heart (1,41,42), but the exact molecular composition of cardiac $I_{Cl,swell}$ remains unknown.

In the present study, we hypothesize that Cav3 prevents membrane damage by upregulating MCC protein abundance and the corresponding $I_{Cl,swell}$. To test this hypothesis, we used HEK293 cells transfected with Cav3 to determine its effect on membrane integrity under extreme hypotonic conditions, MCC expression, and $I_{Cl,swell}$ activity. We performed Förster resonance energy transfer (FRET)-based analysis to evaluate whether the association of Cav3 and various MCCs was dependent on cell stretch and/or caveola integrity. Our findings indicate that Cav3-positive HEK293 cells are highly resistant to extreme hypotonic conditions compared with native (Cav3-negative) HEK293 cells. This enhanced resistance to swelling-induced membrane damage was significantly decreased by incubation with 4-[(2-butyl-6,7-dichloro-2-cyclopentyl-2,3-dihydro-1-oxo-1H-inden-5-yl) oxy]butanoic acid (DCPIB), an $I_{CL,swell}$ inhibitor. Our findings were recapitulated in freshly isolated mouse ventricular cardiomyocytes. We then showed that Cav3 expression in HEK293 cell lines leads to a twofold increase in an endogenous $I_{Cl,swell}$ current and upregulation of caveola structure density, which was accompanied by a significant increase in SWELL1 protein abundance, with no changes in ClC-3 and ClC-2 expression levels, which supports previous studies indicating SWELL1 channels as the primary contributors to $I_{Cl,swell}$ in HEK293 cell lines (42,43). We found that only SWELL1 had dynamic interactions with Cav3, as indicated by significant changes in Cav3/SWELL1 FRET efficiency during HEK293 cell incubation in hypotonic or methyl-β-cyclodextrin (MβCD) solution, conditions that flatten caveolae in cardiomyocytes, as seen in a previous study (6).

MATERIALS AND METHODS

HEK293 cell culture

Cav3-negative and Cav3-positive HEK293 cell lines were maintained at more than 75% confluency in Dulbecco's Modified Eagle Medium supplemented with 10% fetal bovine serum. Cav3-positive HEK293 cell lines were generously provided by the Dr. Lee L. Eckhardt (University of Wisconsin-Madison). Passage number did not exceed 25.

HEK293 cell stretch imaging and analysis

The day before imaging, HEK293 cells were plated at more than 10% confluency on glass-bottom dishes (MatTek) to obtain isolated cells. Cells were incubated with 37°C isotonic (300 milliosmole [mOsM]) or 1 T (Tyrode's) solution with or without 10 μM DCPIB for 1 h and then incubated at 37°C with extreme hypotonic solution (0 T – distilled water) for 15 min. As a negative control, both cell lines were also incubated with 37°C isotonic solution (1 T) for 15 min. Tyrode's solution contained 140 mM NaCl, 5.4 mM

KCl, 1.2 mM KH_2PO_4, 1 mM $MgCl_2$, 1.8 mM $CaCl_2$, 5 mM HEPES, and 5.5 mM dextrose (pH 7.4) (NaOH). During incubation, images were collected every 15 s using NIS-Elements Viewer and analyzed via NIS-Elements Viewer or ImageJ. As performed in previous studies (44–46), isolated cells were considered to have membrane damage when lysis or membrane blebbing was observed during extreme hypotonic treatment, whereas those that decreased after maximal swelling were considered to be undergoing a regulatory volume decrease (Fig. 1 *A*).

Isolation of mouse ventricular myocytes

All methods and protocols used in this study were approved by the animal care and use committee of the University of Wisconsin-Madison following the Guidelines for Care and Use of Laboratory Animals published by the National Institutes of Health (publication 85-23, revised 1996). All animals used in this study received human care in compliance with the Guide for the Care and Use of Laboratory Animals. Left ventricular myocytes were isolated according to the protocol modified from (47). Adult (8–10 weeks old) C57BL6 male mice were used ($n = 17$). Mice were injected with 100 units of heparin and anesthetized with isoflurane (induced at 3%–5% and maintained at 1%–3%). To ensure an appropriate level of anesthesia, loss of the pain reflex was confirmed. The heart was extracted, cannulated, and perfused with Tyrode's solution (37°C, 4 min). Then the heart was perfused with "low Ca^{2+}" solution for 4 min. "Low Ca^{2+}" solution contained 113 mM NaCl, 4.7 mM KCl, 0.6 mM Na_2HPO_4, 0.6 mM $NaHCO_3$, 1.2 mM $MgS0_4$, 10 mM $KHCO_3$, 30 mM taurine, and 10 mM HEPES containing 10 mM 2,3-butanedione monoxime (pH 7.2) (NaOH). Then the perfusion switched to "low Ca^{2+}" solution containing 0.05 mg/mL Liberase Thermolysin low for 10 min. The left ventricle was removed and placed in modified potassium bromide solution containing 100 mM $KC_5H_8NO_4$, 10 mM potassium aspartate, 25 mM KCl, 10 mM KH_2PO_4, 2 mM $MgSO_4$, 20 mM taurine, 5 mM creatine, 0.5 mM EGTA, 5 mM HEPES, 20 mM dextrose, and 1 mg/mL bovine serum albumin (pH 7.4) (KOH). After resting for 1 min, the ventricle was sliced into small pieces and thoroughly mixed via pipetting over several minutes. Isolated single ventricular myocytes were recalcified to a final 1 mM Ca^{2+} concentration and kept in modified KB solution.

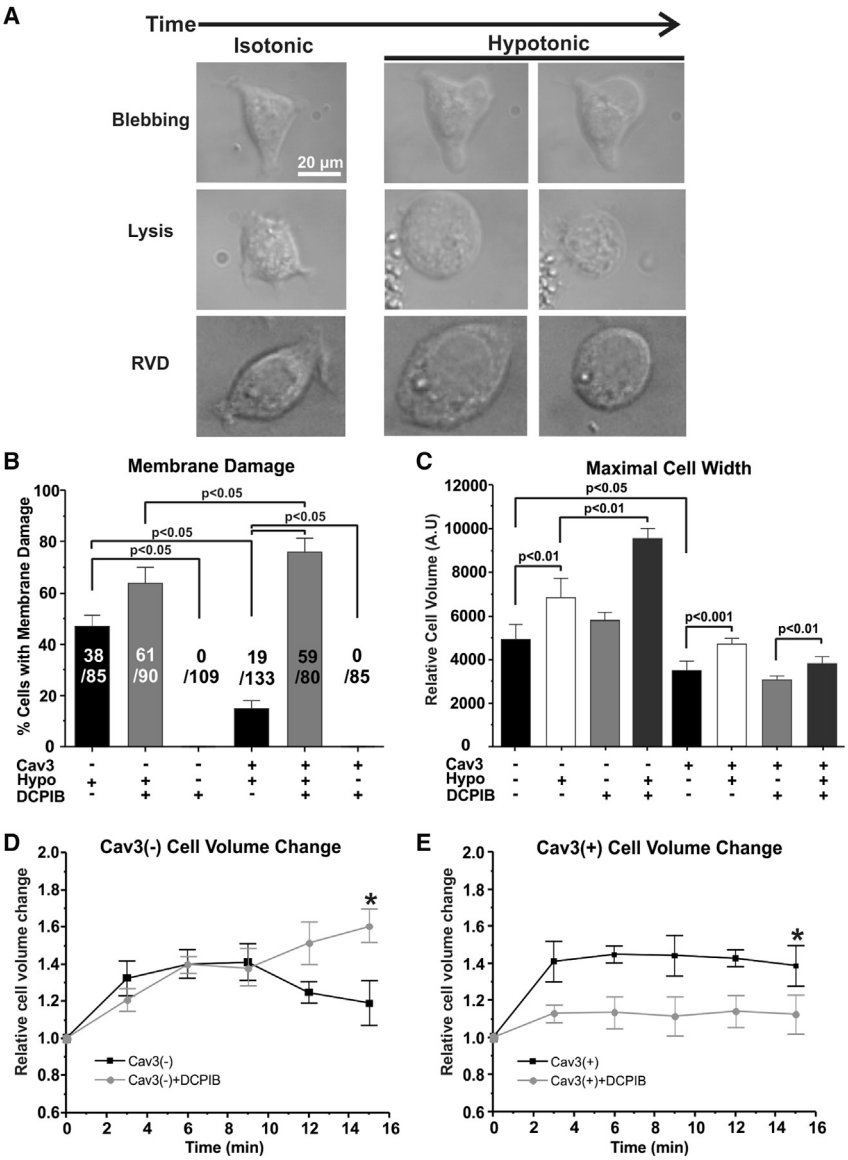

FIGURE 1 Effect of Cav3 expression and DCPIB on membrane damage and relative cell size during hypotonic stress. (*A*) Representative images of Cav3-negative (Cav3(−)) HEK293 cells in isotonic and extreme hypotonic solutions with membrane damage (blebbing or lysis) or undergoing a regulatory volume decrease. (*B*) Percentage of Cav3(−) and Cav3-positive (Cav3(+)) HEK293 cells with membrane damage, treated with 10 µM DCPIB and incubated for 15 min in extreme hypotonic solution. Cav3(+) HEK293 cells were also treated with or without DCPIB and isotonic solution as a negative control. (*C*) Relative minimum and maximum cell size of Cav3(−) and Cav3(+) HEK293 cells treated with 10 µM DCPIB HEK-293 or left untreated under isotonic and extreme hypotonic conditions. $N = 3$ groups, $n = 3$ samples/group. (*D* and *E*) Cav3(−) and Cav3(+) HEK293 cell relative cell volume with extreme hypotonic incubation (Hypo) or extreme hypotonic incubation with 10 µM DCPIB (Hypo + DCPIB) over 15 min *p < 0.05 compared with time 0. $N = 4$–5 groups, $n > 5$ cells/group. p Values within cell types were calculated with paired Student's *t*-tests. p Values between cell types were calculated with one-way ANOVA. Mean ± SE.

Cardiomyocyte cell stretch imaging and analysis

Freshly isolated cardiomyocytes were plated on laminin-coated MatTek dishes for 30–40 min to allow cell attachment. To disrupt caveolae, a portion of cardiomyocytes was pretreated with 10 mM MβCD for 30 min (6,48). The experimental protocol included incubation with isotonic Tyrode's (300 mOsM or 1 T Tyrode's) solution with or without 10 μM DCPIB for 30 min and then moved to the recording stage. Cell images were recorded at the baseline and after application of high hypotonic solution for 20 min (0.1 T). Imaging was performed on a Nikon microscope using NIS-Elements Viewer. Cell analysis was performed in ImageJ. Isolated cells were considered to have membrane damage when lysis or membrane blebbing was observed during high hypotonic treatment (Fig. 2 *A*).

CBM analysis

CBMs were identified based on the following motifs: ΦXXXXΦXXΦ, ΦXΦXXXXΦ, and ΦXΦXXXXΦXX, where Φ is an aromatic amino acid and X is a nonaromatic amino acid (17). In brief, Python was used to convert protein amino acid sequences into binary and scanned for these motifs (the Python script is available at https://figshare.com/articles/journal_contribution/Amino_Acid_Conversion_for_Searching_for_Caveolin-Binding_Domains_/19141901).

FRET transfections and imaging

Caveolin-3-green fluorescent protein (Cav3-GFP, generously provided by Dr. Timothy J. Kamp, University of Wisconsin-Madison), pCAG-GFP (Addgene), and MCC-mCherry (Vectorbuilder) plasmids were transiently transfected into Cav3-negative HEK293 cell lines using Lipofectamine 3000 (Thermo Fisher Scientific) as specified by the protocol. Cell confluency for transfections did not exceed 25%. Prior to imaging, transfected HEK293 cells were incubated with 1 T solution for 30 min at 37°C. After isotonic imaging, HEK293 cells were incubated in mild hypotonic (220 mOsM or 0.7 T) solution for 30 min or for 1 h in 10 mM MβCD 1 T solution with or without 6.5 μM cholesterol (as a positive control). Images were collected using a Leica SP5 confocal microscope system under a ×63 oil immersion objective and analyzed using the Leica Sensitized Emission

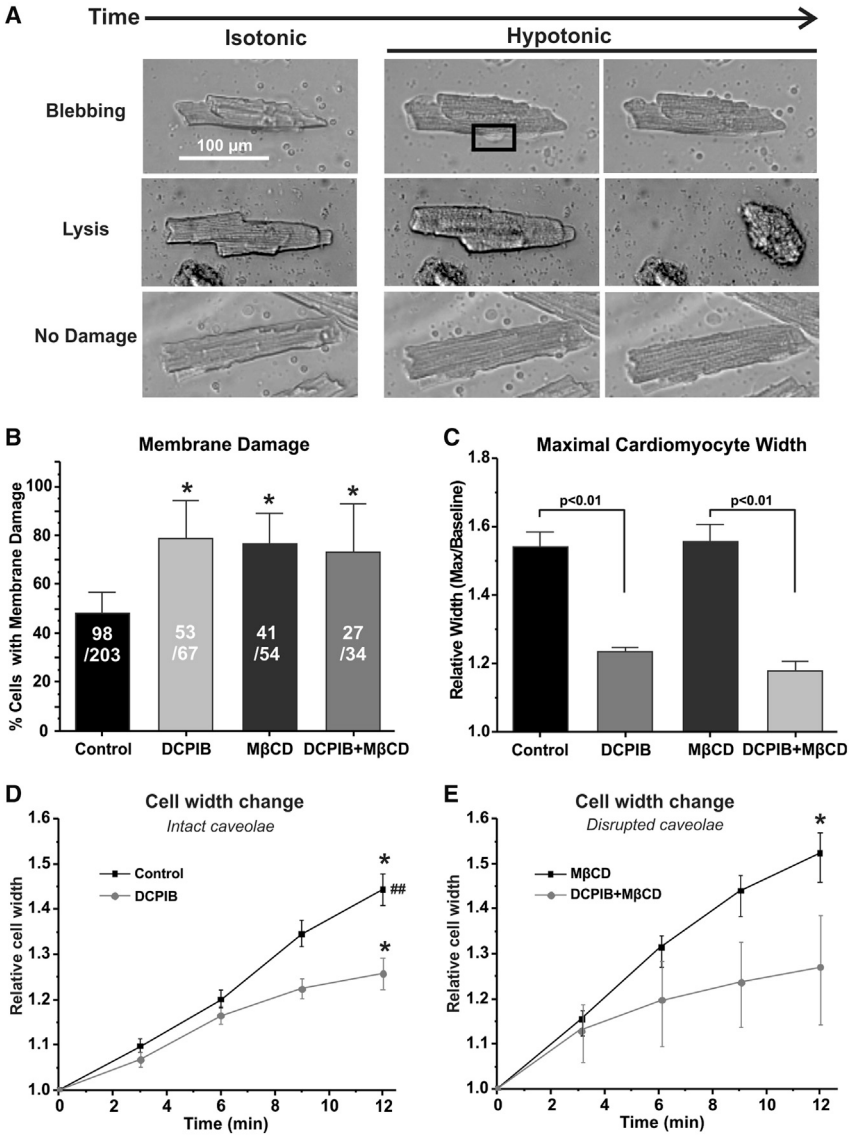

FIGURE 2 Effect of DCPIB and MβCD on swelling-induced membrane damage and cell width in cardiomyocytes. (*A*) Representative images of isolated mouse ventricular myocytes in isotonic (1 T) and highly hypotonic solutions (0.1 T) with membrane damage (blebbing or lysis) or no damage. (*B*) Percentage of isolated mouse ventricular myocytes with membrane damage, treated with 10 μM DCPIB and/or 10 mM MβCD and incubated for 20 min in highly hypotonic solution. *p $<$ 0.05 compared with control (0.1 T). (*C*) Relative maximum width of isolated mouse ventricular myocytes treated with 10 μM DCPIB and/or 10 mM MβCD under highly hypotonic conditions. (*D* and *E*) Relative cell width of isolated mouse ventricular myocytes incubated with high hypotonic solution supplemented with 10 μM DCPIB and/or 10 mM MβCD over 12 min. *p $<$ 0.05 compared with time 0, ##p $<$ 0.05 between the same time points. $N = 3$–5 groups, $n = 3$–10 cells/group. Membrane damage p values were calculated using a one-way ANOVA Kruskal-Wallis test. All other p values were determined via one-way ANOVA. Mean ± SE.

Wizard. In short, the software calculates FRET using the following equation: $E_A(i) = (B-(A^* \beta) - C^*(\gamma - \alpha^*\beta))/(C^*(1- \beta^*\delta))$, where A is the donor channel, B is the FRET channel, C is the acceptor channel, $\alpha = A/C$ (cross-excitation cross-talk), $\beta = B/A$ (donor cross-talk), $\gamma = B/C$ (acceptor cross-excitation), and $\delta = A/B$ (FRET cross-talk) (49). GFP excitation and emission detection was set for 488 nm and 505–515 nm, respectively, and mCherry excitation and emission detection was set for 568 nm and 605–615 nm, respectively.

Whole-cell patch-clamp electrophysiology

Patch-clamp experiments were carried out in the whole-cell configuration. Recordings were performed at room temperature using the Axopatch 200 B amplifier (Axon Instruments, Foster City, CA) with pCLAMP 10.7 software. Recording pipettes were pulled from thin-walled borosilicate glass capillaries (World Precision Instruments, Sarasota FL) with a pipette resistance of 3–5 MΩ. The recordings were filtered at 2 kHz and digitized at 20 kHz. For $I_{Cl,swell}$ measurements, isotonic (1 T Tyrode's solution, 300 mOsM/kg H_2O) bath solution contained 90 mM N-methyl-D-glucamine-chloride, 3 mM $MgCl_2$, 10 mM HEPES, 10 mM glucose, 5 mM CsCl, 0.5 mM $CdCl_2$, 91.9 mM mannitol (pH 7.4) (CsOH) (1). Hypotonic (0.7 T Tyrode's solution) bath solution was made by removing mannitol from the isotonic solution. The pipette solution for HEK293 cells contained 110 mM Cs-methansulfonate, 20 mM CsCl, 2.5 mM MgATP, 8 mM EGTA, 0.1 mM $CaCl_2$, 10 mM HEPES (pH 7.1) (CsOH). 10 μM DCPIB (Tocris) was added to hypotonic solution to inhibit $I_{Cl,swell}$. Whole-cell currents were recorded from a holding potential of −60 mV with 300-ms test pulses from −100 to 60 mV in 10-mV increments. Data were analyzed using Microcal Origin software (OriginLab, Northampton, MA, USA).

Western blot

Cav3-negative and Cav3-positive HEK293 cell lines were collected at 70% confluency with CHAPS lysis buffer (150 mM NaCl, 50 mM Tris-HCl, 0.5% CHAPS, 1× protease inhibitor (Bimake)). Using bicinchoninic acid assays to determine protein concentration, 10μg of protein was loaded to each gel (Bio-Rad, 4%–20% Tris-glycine) lane to not exceed the quantifiable range of glyceraldehyde 3-phosphate dehydrogenase (GAPDH). Gels were transferred to polyvinylidene fluoride (PVDF) via the Powerblotter system (Invitrogen) set for mixed-range molecular mass. Membranes were blocked for 1 h at room temperature with 3% non-fat milk and incubated overnight (∼16 h) with a primary antibody (1:500–1:1000) at 4°C. Corresponding Alexa Fluor-488 fluorescent secondary antibodies were used to evaluate protein expression. Primary antibodies for Cav3 (rabbit polyclonal; ab2912, Abcam), ClC-2 (goat polyclonal; SAB2501373, Sigma-Aldrich), ClC-3 (rabbit polyclonal; ACL-001, Alomone Labs), and GAPDH (mouse monoclonal, G8795, Millipore Sigma) have been validated previously (1). SWELL1 (rabbit polyclonal; SAB2108060, Sigma-Aldrich) antibody validation is provided under Results.

Electron microscopy

Samples were immersion fixed in 2.5% glutaraldehyde, 2.0% paraformaldehyde buffered in 0.1 M sodium cacodylate buffer (CB) for 2 h at room temperature. The primary fixed samples were rinsed five times for 5 min each in CB, post-fixed in 1% osmium tetroxide and 1% potassium ferrocyanide in 0.1 M CB for 1 h at room temperature, and rinsed in CB as before. Dehydration was performed in a graded ethanol series (35%, 50%, 70%, 80%, and 90% for 5 min each step; 95% for 10 min; and 100% for 3 × 10 min) and then transitioned in propylene oxide twice for 7 min each. Fully dehydrated samples were infiltrated in increasing concentrations of PolyBed 812 (Polysciences, Warrington, PA) and propylene oxide. Embedding and polymerization took place in fresh PolyBed 812 for 24 h at 60°C. The glass coverslips were etched away with hydrofluoric acid and rinsed. The samples were sectioned on a Leica EM UC6 ultramicrotome at 100 nm. The sections were collected on formvar-coated 300-mesh slot Cu grids (EMS, Hatfield, PA) and post-stained with uranyl acetate and lead citrate. The sectioned samples were viewed at 80 kV on a Philips CM120 transmission electron microscope equipped with a BioSprint12 digital camera (AMT Imaging Systems, Woburn, MA). Caveolae were defined as omega-shaped invaginations (open caveolae) or proximal subsarcolemmal vesicles (closed caveolae) with a 50- to 100-nm diameter (6–8).

Co-immunoprecipitation

HEK293 cell line lysates were obtained using the aforementioned method, and immunoprecipitation was carried out using 5 μg of anti-Cav3 or anti-SWELL1 antibodies; control immunoglobulin G was used at the same concentrations as the specific antibodies as a negative control. Briefly, HEK293 cell lysates were incubated with antibodies for 2 h at 4°C and an additional 2 h at 4°C with protein A and protein G magnetic Sepharose beads (Cytiva). The flowthrough was collected for downstream analysis, and the beads were washed three times with simple lysis buffer (150 mM NaCl, 50 mM Tris-HCl). Proteins were then eluted using 2.5% acetic acid and then again with 4× Laemmli buffer containing dithiothreitol and sodium dodecyl sulfate at 50°C for 10 min. Immune complexes were analyzed by Western blot as described above by probing with antibodies specific for SWELL1, Cav3, and GAPDH (as a negative control).

qRT-PCR

Total RNA was extracted from HEK293 cell line lysates using TriZol reagent (Invitrogen). Quantitative reverse transcription polymerase chain reaction (qRT-PCR) with probes targeting *LRRC8A*, *Cav3*, and *GAPDH* was performed using TaqMan Fast Advanced Master Mix (Thermo Fisher Scientific). Levels of messenger RNA (mRNA) were quantified using the ΔΔCt method and normalized to the housekeeping gene *GAPDH*.

Statistics

Paired Student's *t*-test was used to evaluate the significance of FRET measurements. Unpaired Student's *t*-test was used to evaluate the significance of qPCR, caveola expression, and Western blot experiments between HEK293 cell types. One-way analysis of variance (ANOVA) was used to determine significance in cell swelling experiments. Unpaired Student's *t*-test and one-way ANOVA with Bonferroni correction were used for patch-clamp data. All statistical analyses were performed using GraphPad Prism 5 (GraphPad Software) or Origin 6.1 (OriginLab). $p < 0.05$ was considered statistically significant. Values were presented as mean ± standard deviation (SD) or mean ± standard error (SE), as indicated.

RESULTS

Cav3 reduces membrane damage in HEK293 cells

It has been reported previously that Cav3 and MCCs have a mechanoprotective role (24,25,50–52). Although Cav3 has been implicated in regulating MCCs, it has not been directly shown how this translates into cellular mechanoprotection (1). To verify that Cav3 improves membrane resistance to hypotonic solution-induced stretch, we first evaluated the membrane damage rate of Cav3-negative and Cav3-positive HEK293 cell lines in extreme hypotonic solution (<20 mOsM) by monitoring cell morphology over the

course of 15 min (Fig. 1 *A*). We found that Cav3-positive HEK293 cells were significantly more resistant to cell swelling-induced membrane damage, with an average membrane damage rate of 14.7% ± 2.4% compared with a 46.7 ± 4.3% rate for Cav3-negative HEK-293 cells ($p < 0.05$) (Fig. 1 *B*). To determine the contribution of $I_{Cl,swell}$ to this difference, we pre-incubated both cell groups with 10 μM DCPIB (an $I_{Cl,swell}$ inhibitor) before applying extreme hypotonic solution. We found a significant increase (by approximately fivefold, $p < 0.05$) in Cav3-positive cell membrane damage and a significant increase (1.4-fold, $p < 0.05$) for Cav3-negative HEK293 cells (Fig. 1 *B*). This indicates that the mechanoprotection provided by Cav3 may be associated with enhanced volume-regulated anion channel activity in Cav3-positive HEK293 cells. As a negative control, we incubated both cell types with isotonic (300 mOsM) solution with and without 10 μM DCPIB for 1 h and observed no membrane damage (Fig. 1 *B*).

Cav3 expression and DCPIB treatment also had a significant effect on relative isotonic cell size and overall swelling size. We found that Cav3-positive HEK293 cells were ∼29% smaller compared with Cav3-negative under isotonic conditions ($p < 0.05$) and ∼31% smaller under hypotonic conditions ($p < 0.001$), on average (Fig. 1 *C*). Because the swelling-induced volume of Cav3-positive HEK293 cells is still smaller than that of Cav3-negative HEK293 cells, we speculate that this smaller size is not due to extra caveolae increasing membrane convolution but possibly due to metabolic load induced by the Cav3-encoding plasmid and/or the selective agent G418 (53). DCPIB-treated Cav3-positive HEK293 cells were ∼19% smaller ($p < 0.05$) under hypotonic conditions compared with untreated Cav3-positive cells (Fig. 1, *C* and *E*). DCPIB may negate a regulatory volume decrease in Cav3-negative HEK293 cells, causing them to continue to increase in size (Fig. 1 *D*; $p < 0.05$) and completely abolishes changes in relative cell volume for Cav3-positive HEK293 cells (Fig. 1 *E*; $p < 0.05$). We speculate that, because $I_{Cl,swell}$ is largely involved in the regulatory volume decrease, it is possible that DCPIB also activates and inhibits various K2P potassium channels, such as TREK, TRAAK, and TRESK channels, that may be enriched in Cav3-positive HEK293 cells, causing the overall decrease in swelling-induced volume change observed (27,54).

To provide cardiac relevance to our HEK293 findings, we performed similar cell swelling experiments on isolated mouse ventricular myocytes. We found that during a 20-min swelling condition, the average percentage of cardiomyocytes with membrane damage increased from 60% for control to 95% for DCPIB-treated cardiomyocytes (Fig. 2 *B*; $p < 0.05$). This baseline resistance to membrane damage was abolished with MβCD treatment (95% membrane damage rate; Fig. 2 *B*; $p < 0.05$). These findings indicate an equivalent role of caveola membrane structures and caveola-associated $I_{Cl,swell}$ in facilitating resistance to mechanical membrane damage in cardiomyocytes. Similar to HEK293 data, DCPIB pre-treatment significantly reduced the relative maximal swelling width (Fig. 2 *C*; $p < 0.01$) and swelling width change (Fig. 2, *D* and *E*; $p < 0.05$) of isolated cardiomyocytes. In contrast to HEK293 cells, control isolated cardiomyocytes exhibited no regulatory volume decrease in response to high hypotonic solution.

Cav3 expression increases caveolae abundance in HEK293 cells

As expected, Cav3 expression significantly increased the average number of caveolae, including closed, open, and total caveolae, in Cav3-positive HEK293 cells (Fig. 3 *A*) by ∼40% compared with Cav3-negative HEK293 cells ($p < 0.05$; Fig. 3 *B*). However, because Cav3-positive cells have a 25% shorter relative cell perimeter compared with Cav3-negative cells ($p < 0.001$; Fig. 3 *C*), Cav3-negative HEK293 cells may have additional caveolae because of cell size. To factor this, we corrected the average number of caveolae in Cav3-positive cells by the difference in cell perimeter between the two cell types and found that Cav3-positive HEK293 cells may have ∼90% more caveolae per cell compared with Cav3-negative cells ($p < 0.001$; Fig. 3 *D*).

MCCs are predicted to interact with Cav3

To determine which MCC may interact with Cav3, we performed a CBM analysis. Caveolar proteins may directly interact with a highly conserved 20-residue sequence of the caveolin scaffolding domain located in the membrane-proximal N terminus of Cav3 (Fig. 4 *A*). This interaction is achieved via a CBM composed of a series of specifically spaced aromatic residues (ΦXΦXXXXΦ, ΦXXXXΦXXΦ, or ΦXΦXXXXΦXX and their reciprocals, where Φ is tyrosine (Y), phenylalanine (F), or tryptophan (W), and X is any other amino acid) (17). Caveolin binding domain analysis revealed three possible CBMs within SWELL1 located in extracellular loop 1 and transmembrane region 2 and in the C-terminal cytosolic region (Fig. 4 *C*). Analysis of ClC-2 (Fig. 4 *D*) and ClC-3 (Fig. 4 *E*) revealed one CBM in each protein in membrane region 9 and extracellular loop 1, respectively. CBM analysis of the control proteins revealed one CBM in GAPDH and none in actin cytosolic proteins as well as none in $K_v11.1$ (hERG) K^+ sarcolemmal non-caveolar (Fig. 4 *E*) (55) membrane protein. These findings indicate that SWELL1 is the most likely to interact with Cav3 via a CBM and, thus, likely to be associated with caveola structures.

Cav3 increases SWELL1 abundance

To determine the molecular composition that underlies $I_{Cl,swell}$ augmentation in Cav3-positive HEK293 cells, we

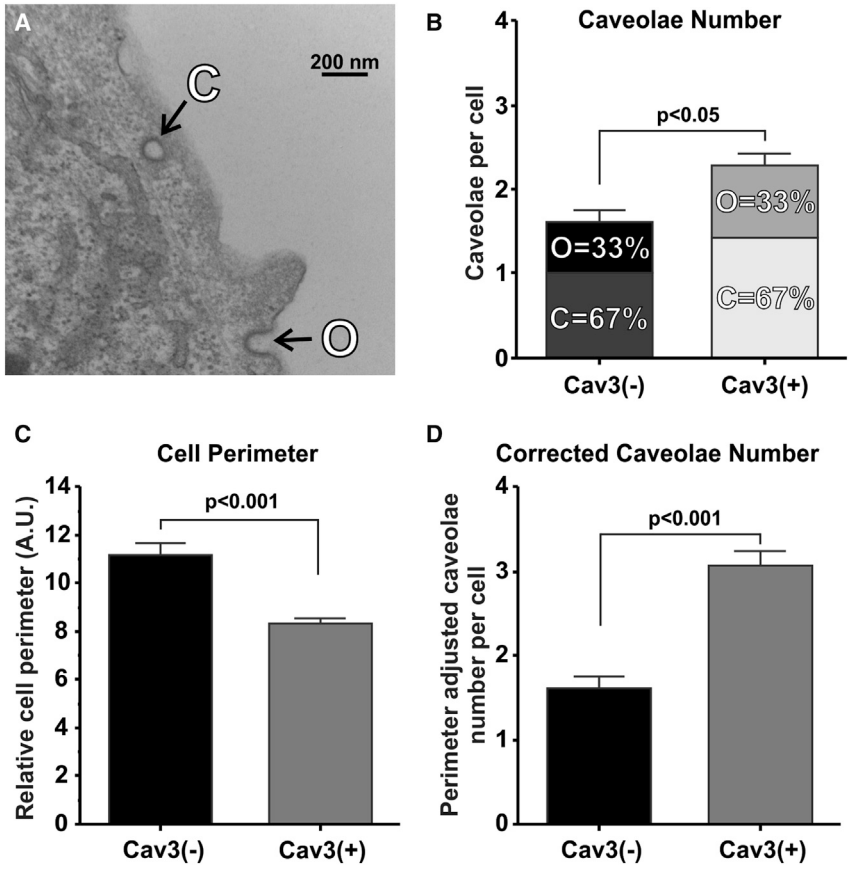

FIGURE 3 Cav3 expression increases caveolae abundance in HEK293 cells. (*A*) Representative image of Cav3(+) HEK293 cells with closed and open caveolae. (*B*) Average number of open, closed, and total caveolae per cell in Cav3(−) and Cav3(+) HEK293 cells. $N = 4$ samples, $n = 30$ cells/sample. (*C*) Average relative Cav3(−) and Cav3(+) HEK293 cell perimeter in arbitrary units. $N = 4$ samples, $n = 10$–20 cells/sample. (*D*) Average number of total caveolae per cell in Cav3(−) and Cav3(+) HEK293 cells, corrected by average relative cell perimeter. $N = 4$ samples, $n = 30$ cells/sample. Mean ± SE. Caveolae number p values were calculated with unpaired Student's *t*-test. Relative cell perimeter p value was determined via Welch's t test. Mean ± SE.

performed Western blot on both cell types to determine possible changes in MCC protein abundance. We first confirmed SWELL1 antibody specificity via small interfering RNA (siRNA) knockdown (Fig. 5, *A* and *B*). In Cav3-positive cells, Western blot demonstrated a twofold increase in SWELL1 protein abundance, whereas ClC-2 and ClC-3 protein levels were unchanged (Fig. 5 *C*, E1–E3), indicating that the increase in $I_{Cl,swell}$ current is due to upregulation of the SWELL1 protein expression level. Interestingly, qPCR measurements did not show any significant change in *SWELL1* mRNA availability relative to *GAPDH* in Cav3-positive versus Cav3-negative HEK293 cells (Fig. 5 *D*). We used co-immunoprecipitation to dissect the possible physical coupling between Cav3 and SWELL1. Co-immunoprecipitation analysis of SWELL1 and Cav3 demonstrated reciprocal pulldown (Fig. 5 *F*), which confirms a close association between Cav3 and SWELL1 proteins observed in CBM and FRET experiments.

Cav3 expression increases $I_{Cl,swell}$ density in HEK293 cells

To determine the molecular mechanisms by which Cav3-positive HEK293 cells resist swelling-induced membrane damage, we performed patch-clamp experiments to evaluate changes in $I_{Cl,swell}$ current activity. As expected, we also found significant upregulation of $I_{Cl,swell}$ in Cav3-positive HEK293 cells (Fig. 6). Cav3 expression up-regulated inward and outward components of $I_{Cl,swell}$ current at testing potentials from −100 to +60 mV. $I_{Cl,swell}$ normalized to cell capacitance at −100 mV in Cav3-positive cells was significantly larger (-25.9 ± 3.4 pA pF^{-1}, $n = 9$, $p < 0.05$) compared with Cav3-negative cells (-14.6 ± 2.2 pA pF^{-1}, $n = 8$; Fig. 4 *D*). $I_{Cl,swell}$ at +60 mV in Cav3-positive cells was significantly bigger (47.6 ± 6.6 pA pF^{-1}, $n = 9$, $p < 0.05$) in comparison with Cav3-negative cells (27.6 ± 4.2 pA pF^{-1}, $n = 8$; Fig. 6 *D*). These findings, coupled with the cell swelling experiments, demonstrate that Cav3 expression significantly augments $I_{Cl,swell}$ activity and suggests that this change may play a crucial role in promoting cellular resistance to swelling-induced membrane damage.

Cav3/MCC interaction FRET analysis

As performed similarly in previous studies (56,57), to determine the functional interaction between MCCs and Cav3 under conditions where caveolae may be disrupted by mechanical or chemical forces, we used Cav3-negative HEK293 cells transfected with Cav3-GFP (or pCAG-GFP as a negative control) and SWELL1-, ClC-2-, or ClC-3-mCherry. Sensitized emission FRET analysis was used to

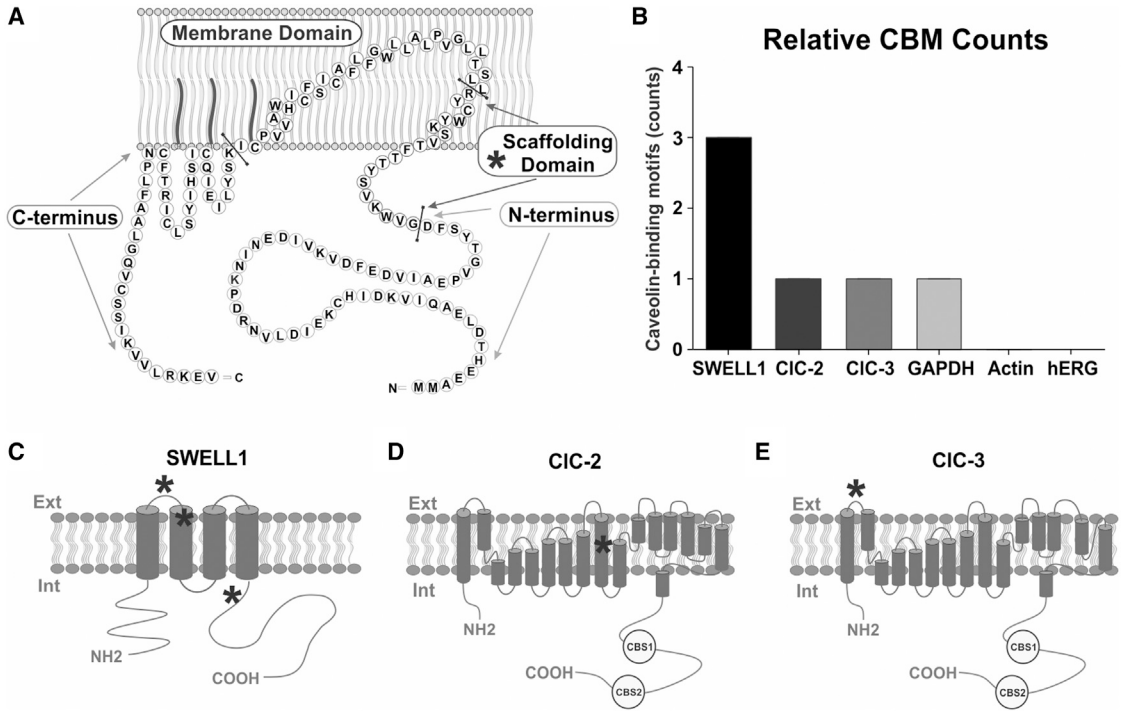

FIGURE 4 CBMs for MCCs. (*A*) Structure of the caveola scaffolding protein caveolin-3. Caveolin-3 has four primary domains: NH2-terminal domains; scaffolding domains that form α-helices and are inserted into the membrane, with a cholesterol recognition/interaction amino acid consensus composed of the eight residues proximal to the membrane domain; helix-turn-helix membrane domains; and COOH-terminal domains. Bars indicate separation of protein domains. From Busija et al. (75) with permission. (*B–D*) Location of possible CBMs (shown by asterisks) within SWELL1, ClC-2, and ClC-3 protein structures. CBS, cystathionine β synthase. (*E*) CBM counts relative to non-caveola-associated proteins.

evaluate the dynamics of these interactions in response to changes in membrane tension and caveola integrity. The presence of a FRET signal between pCAG-GFP and SWELL1-, ClC-2-, and ClC-3-mCherry confirms membrane localization of all three MCC-mCherry variants (Figs. 7 and 8). A subsequent FRET signal between Cav3-GFP and MCC-mCherry variants on the cell periphery indicates Cav3-GFP membrane localization. The observed Cav3-SWELL1 FRET efficiency sensitivity to caveola disruption (Fig. 10), also found in Konig et al. (58), indicates Cav3-GFP membrane localization. Colocalization analysis (Fig. 9) demonstrated limited membrane colocalization for all FRET probe combinations, with the highest total colocalization (M1 and M2) between Cav3-GFP and SWELL1-mCherry. Under isotonic conditions, the FRET efficiency for Cav3-GFP and all MCCs was between 0.2 and 0.5 (corresponding to an interprotein distance of 4–8 nm), which indicates a close proximity of the channel proteins to Cav3 and, therefore, is within the structural dimension of caveola nanodomains of 50–100 nm (5).

To activate MCCs, we applied mild (220 mOsM) hypotonic swelling from relative osmolality of 1 T (isotonic) to 0.7 T (hypotonic). Cav3-GFP and SWELL1-mCherry FRET efficiency had a reported average of 0.5 (4 nm interprotein distance) (Fig. 10 *A*1). Upon hypotonic incubation, the average FRET efficiency was significantly decreased to 0.3 (6 nm) (Fig. 10 *A*1), which was similar to the negative control average FRET efficiency between pCAG-GFP (membrane-bound GFP) and SWELL1-mCherry was 0.3 (6 nm) for isotonic and hypotonic conditions (Fig. 10 *A*2). The average intracellular Cav3/SWELL1 FRET was similar to negative control FRET and not significantly changed between isotonic and hypotonic conditions (Fig. 10 *A*3).

Interestingly, the Cav3/ClC-2 (Fig. 10 *B*1) and Cav3/ClC-3 (Fig. 10 *C*1) average FRET efficiency was unchanged at 0.2 (8 nm) and 0.4 (5 nm), respectively, between isotonic and hypotonic conditions. The pCAG/ClC-2 (Fig. 10 *B*2) and pCAG/ClC-3 (Fig. 10 *C*2) average FRET was higher than the experimental counterparts and not significantly changed between isotonic and hypotonic conditions at 0.4 and 0.5, respectively, indicating that these channels are no more associated with Cav3 than a common membrane protein.

To evaluate whether the swelling-induced decrease in Cav3/SWELL1 FRET was due to caveola disruption, we treated HEK293 cells transfected with Cav3-GFP and SWELL1-mCherry with MβCD (a cholesterol solubilizer). Similar to hypoosmotic swelling, treatment with MβCD resulted in an average FRET efficiency reduction from 0.4 to 0.2 (Fig. 10 *D*1). This change in Cav3/SWELL1 FRET was not observed when incubated with cholesterol solubilized MβCD, acting as a negative control (Fig. 10 *D*2). As expected, treatment with MβCD had no significant effect on

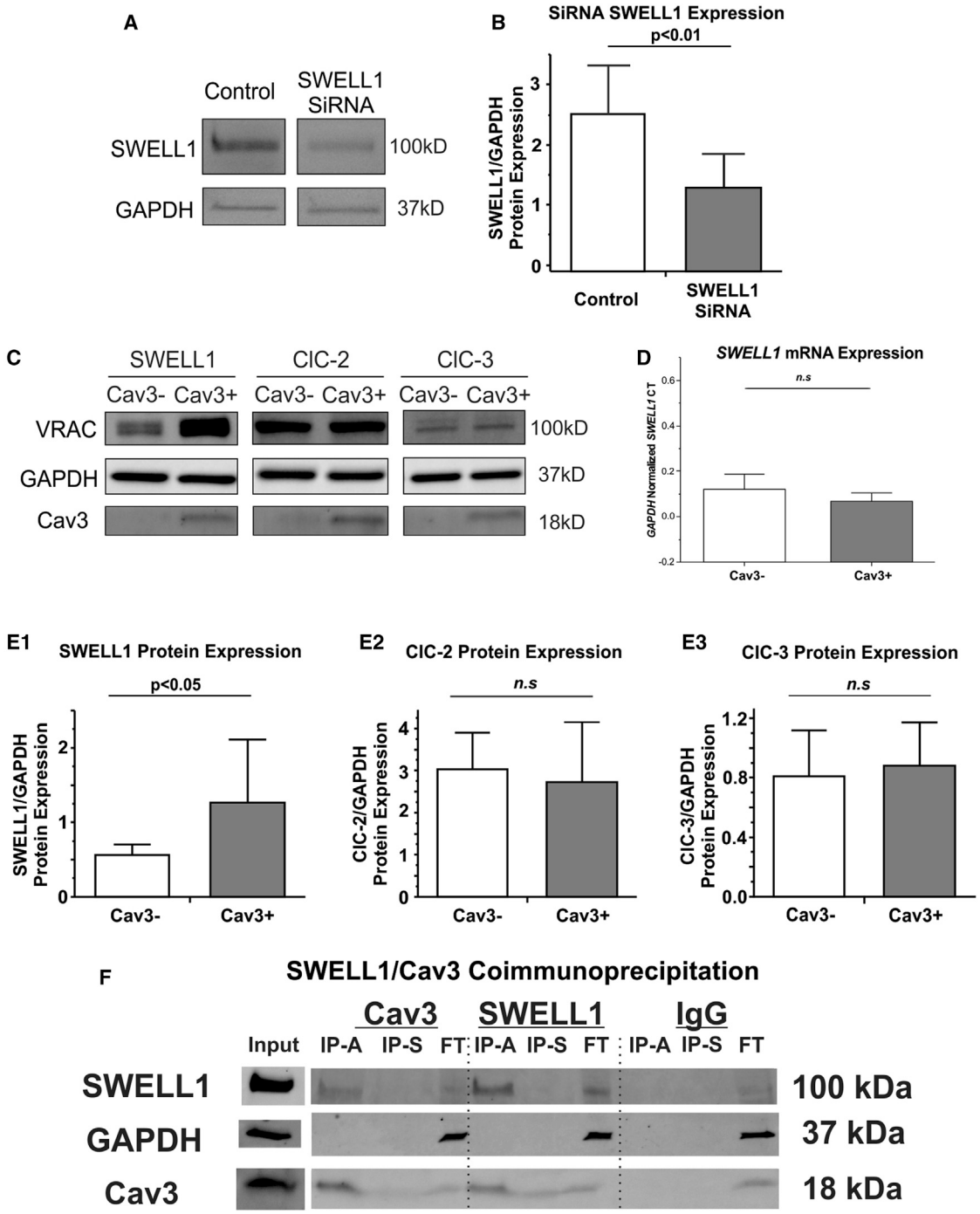

FIGURE 5 Effect of Cav3 on MCC protein expression in HEK293 cells. (*A*) SWELL1 antibody (rabbit polyclonal; SAB2108060, Sigma-Aldrich) validation, showing representative Western blots of SWELL1 with/without siRNA treatment; other antibodies have been validated previously (2). (*B*) Quantification of SWELL1 siRNA relative to GAPDH. (*C*) Representative Western blots of MCCs, GAPDH, and Cav3 in Cav3(−) and Cav3(+) HEK293 cell lines. (*D*) qPCR *SWELL1* CT quantification relative to *GAPDH* with and without Cav3 expression. (*E1–E3*) Quantification of MCC protein expression with and without Cav3 expression. (*F*) Co-immunoprecipitation of SWELL1 and Cav3 in Cav3(+) HEK293 cell lines. IP-A, immunoprecipitation via 2.5% acetic acid; IP-S, immunoprecipitation via sodium dodecyl sulfate; FT, flowthrough. $N = 3$ groups, $n = 3$–7 samples/group. Mean ± SD. p Values were determined by unpaired Student's *t*-tests. n.s., non-significant.

intracellular Cav3/SWELL1 FRET (Fig. 10 *D*3). These data suggest that SWELL1 association with Cav3 is dependent on caveola integrity and is at a degree higher than the other MCCs tested.

DISCUSSION

In the present study, we found that Cav3-positive HEK293 cells are significantly and highly resistant to swelling-induced

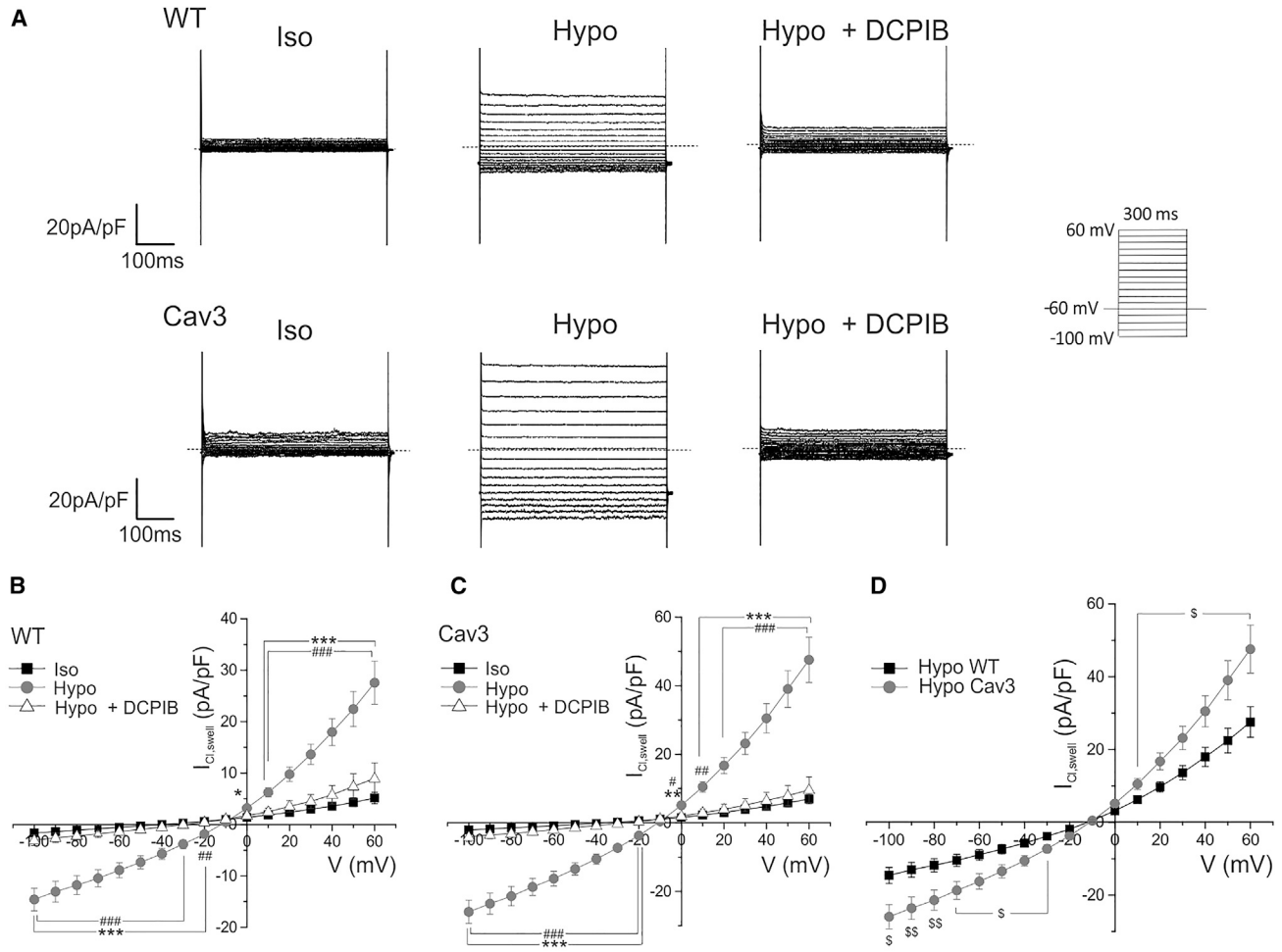

FIGURE 6 Cav3 increases $I_{Cl,swell}$ density in HEK293 cells. (*A*) Representative current traces illustrating $I_{Cl,swell}$ currents in isotonic (Iso), hypotonic (Hypo), and Hypo with 10 μM DCPIB (Hypo + DCPIB) solutions in Cav3(−) (wild-type) and Cav3(+) HEK293 cells. Whole-cell currents were recorded using the protocol indicated in the inset. (*B–D*) Mean current-voltage relationships of peak $I_{Cl,swell}$ density in Iso, Hypo, and Hypo + DCPIB solution in Cav3(−) HEK293 cells (*B*) (n = 5–8 cells; ***,*p < 0.001, 0.05 between Hypo and Iso; ###,##p < 0.001, 0.01 between Hypo and Hypo + DCPIB by one-way ANOVA with Bonferroni correction) and Cav3(+) HEK293 cells (*C*) (n = 4–9 cells; ***,**p < 0.001, 0.01 between Hypo and Iso; ###,##,#p < 0.001, 0.01, 0.05 between Hypo and Hypo + DCPIB by one-way ANOVA with Bonferroni correction) as well as a comparison between hypotonically activated $I_{Cl,swell}$ in Cav3(−) versus Cav3(+) HEK-293 cells (*D*) ($$,$p < 0.01, 0.05 between Cav3(+) and Cav3(−) (wild-type) groups by one-way ANOVA with Bonferroni correction).

membrane damage and that this mechanoprotection is partially imparted via $I_{Cl,swell}$ associated with SWELL1 activation. We observed similar effects in mouse ventricular myocytes, where DCPIB and caveola depletion via MβCD increased the percentage of cells with membrane damage. It has been suggested by us and other groups that MCCs form macromolecular complexes within caveolae via their interaction with caveola scaffolding proteins, known as caveolins (1,3). This topic has been explored using CBM analysis to predict caveolin binding (17). However, as shown in the present study, where chloride channels known to associate with caveolae (1) have a similar amount of CBMs with non-membrane control proteins (Fig. 2 *E*) as well as other work questioning the reliability of CBM analysis (59), direct experimentation is required to confirm caveolin-interacting proteins and whether these interactions are sensitive to changes in membrane mechanical or chemical stress that affects caveola integrity. In this study, we demonstrate that, of the MCCs studied, only SWELL1 associates with the muscle-specific caveola scaffolding protein Cav3 at a degree higher than the control membrane protein (pCAG-GFP) and may form a caveolar mechanosensitive complex. Our findings show that SWELL1 is a crucial component of Cav3-associated $I_{Cl,swell}$ and that its abundance is increased via Cav3 expression. We identify a dynamic association between SWELL1 and Cav3 within this mechanosensitive macromolecular complex that is sensitive to caveola disruption via membrane swelling or cholesterol depletion. These data suggest that the mechanoprotection induced by Cav3 expression is partially due to its relationship with SWELL1 within caveolar domains.

Several candidates, including ClC-2, ClC-3, and SWELL1, have been proposed to form $I_{Cl,swell}$ in various cell types

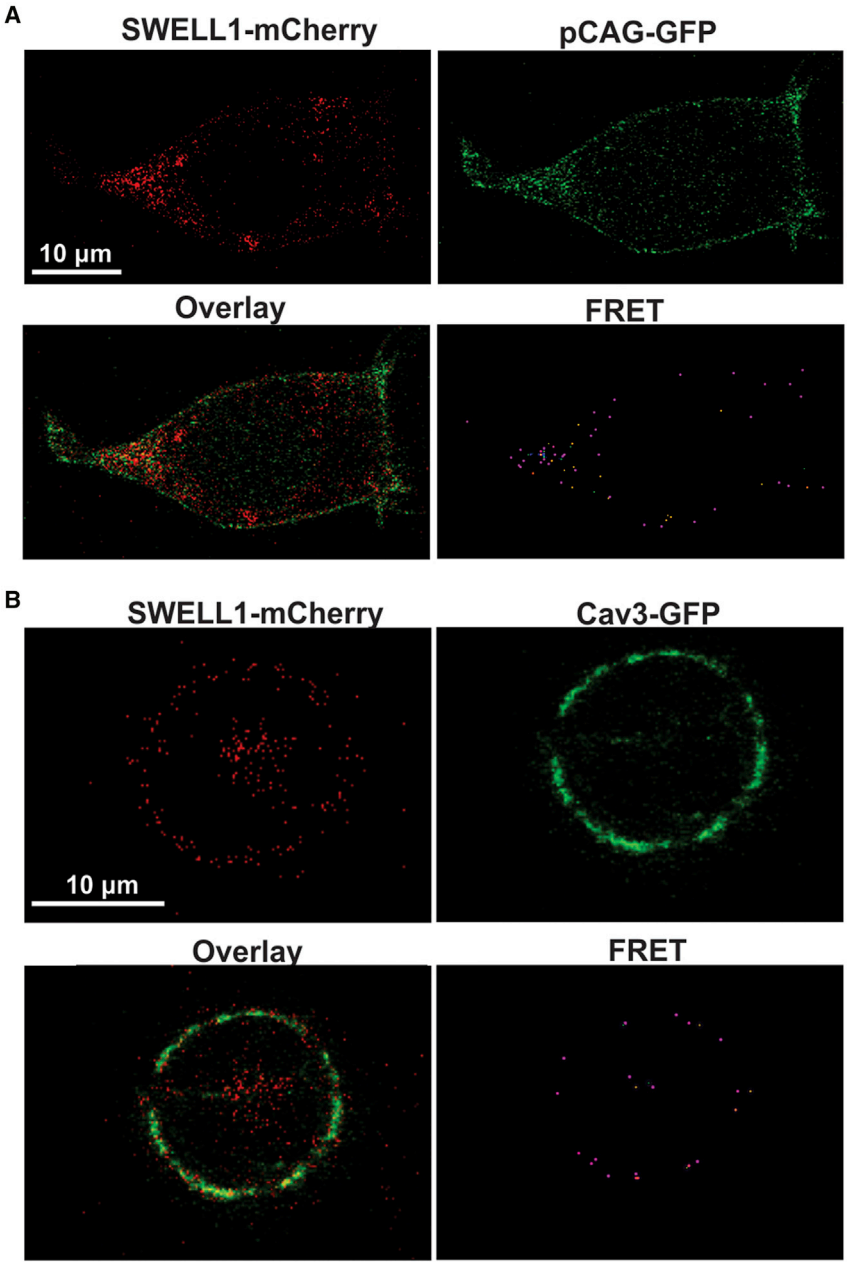

FIGURE 7 Representative images and FRET of HEK293 cells transfected with the pCAG-GFP , Cav3-GFP , and SWELL1-mCherry plasmids. (*A*) pCAG-GFP and SWELL1-mCherry transfections. (*B*) Cav3-GFP and SWELL1-mCherry transfections.

(1,42,43). Studies examining the role of MCCs and $I_{Cl,swell}$ in HEK293 cell lines have shown that SWELL1 is the predominant contributor to $I_{Cl,swell}$ (43). Although SWELL1 mRNA and protein expression as well as its caveolar localization have been detected in the heart, the contribution of these channels to native cardiac $I_{Cl,swell}$ still remains unknown. Although the association between $I_{Cl,swell}$ and caveolins is well documented (1–3,6), our results specifically implicate Cav3 as a major regulator of SWELL1, suggesting a more significant role of the channel in myocytes. This finding is supported by patch-clamp and Western blot results demonstrating that Cav3 transfection upregulates SWELL1 protein abundance, which is translated into elevated hypotonic $I_{Cl,swell}$ activity, but no change in isotonic conditions (Fig. 4). Given these findings and other data (42) showing that SWELL1 knockout in HEK293 cells abolishes $I_{Cl,swell}$, it is likely that SWELL1 channels are mainly responsible for $I_{Cl,swell}$ activity in HEK293 cells. MβCD has been found to evoke $I_{Cl,swell}$ activity (6), whereas MβCD and DCPIB increase the rate of membrane damage in HEK293 cells and mouse ventricular myocytes, as observed in the present study. This may indicate that the two drugs reduce membrane integrity via separate mechanisms.

Because Cav3-negative HEK293 cells lack endogenous Cav3 but do express Cav1 in caveolar fractions, it is plausible that their $I_{Cl,swell}$ is partly generated by SWELL1

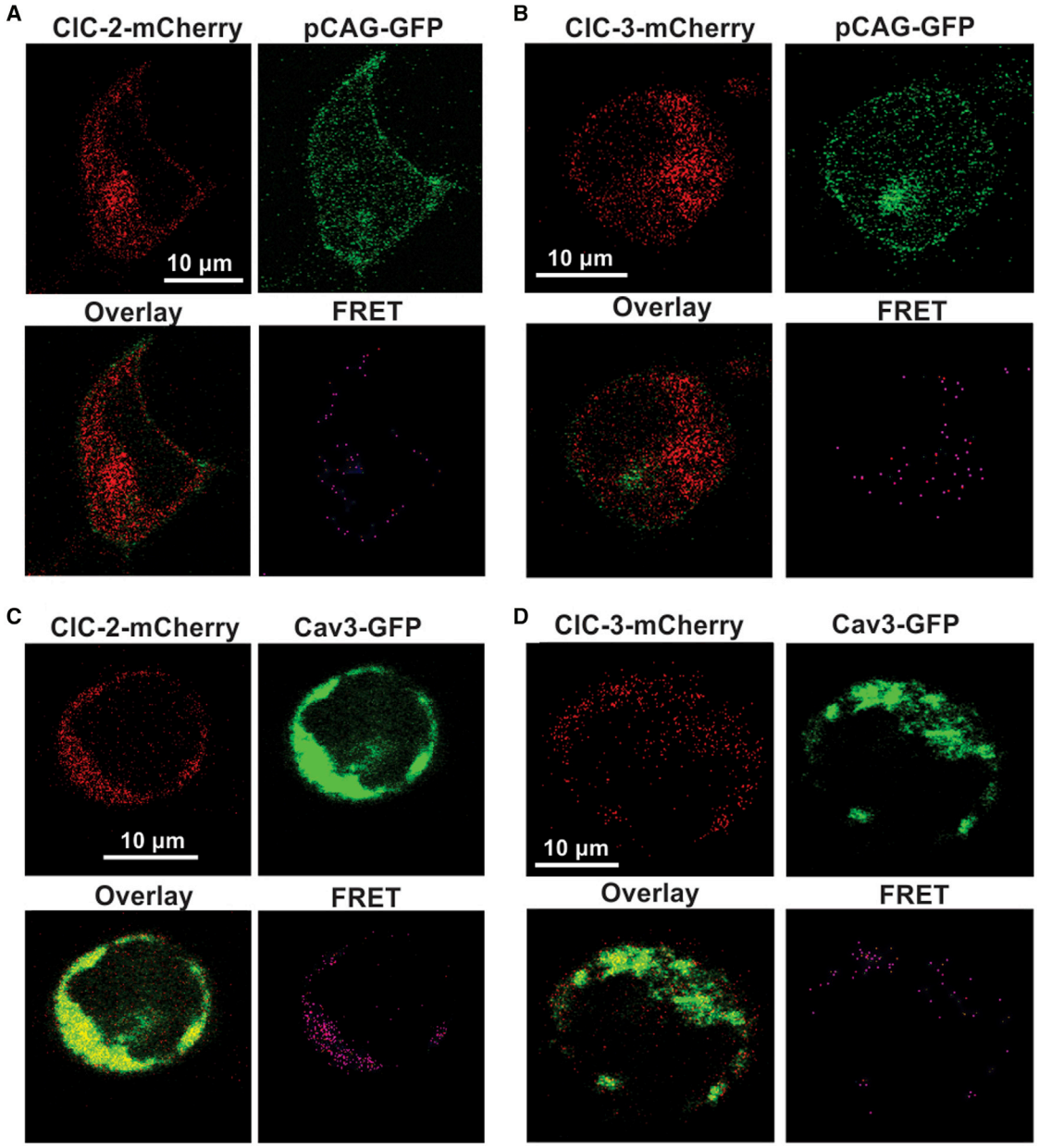

FIGURE 8 Representative images and FRET of HEK293 cells transfected with the pCAG-GFP , Cav3-GFP, ClC-2-mCherry, and ClC-3-mCherry plasmids. (*A*) pCAG-GFP and ClC-2-mCherry transfections. (*B*) pCAG-GFP and ClC-3-mCherry transfections. (*C*) Cav3-GFP and ClC-2-mCherry transfections. (*D*) Cav3-GFP and ClC-3-mCherry transfections.

channels localized within Cav1-generated caveolae. This is further substantiated by Trouet et al. (3), who determined that Cav1 knockout abolishes $I_{Cl,swell}$ and that truncated Cav1 impairs activation of $I_{Cl,swell}$ in another non-muscle cell culture type. Given that atrial tissue expresses Cav1 and Cav3 (60), these findings suggest that both caveolin proteins may play a role in regulating $I_{Cl,swell}$ activity; they have been shown to be involved in various cardiac pathologies, and this indicates that future studies aiming to dissect the contribution of $I_{Cl,swell}$ in various diseases should consider both caveolin proteins when applicable.

Our qPCR data showed no change in SWELL1 mRNA expression with transgenic Cav3 expression despite a significant increase in the corresponding protein level. This disconnect between mRNA expression and protein abundance is fairly common (61) and, in this case, may be due to lipid interactions that stabilize membrane proteins (62,63). it has been demonstrated that Cav3 acts as a chaperone for angiotensin II type 1 receptors by trafficking the receptor via the exocytic pathway for cell membrane localization (64), and heart-specific conditional knockout of Cav3 results in dramatic downregulation of angiotensin II

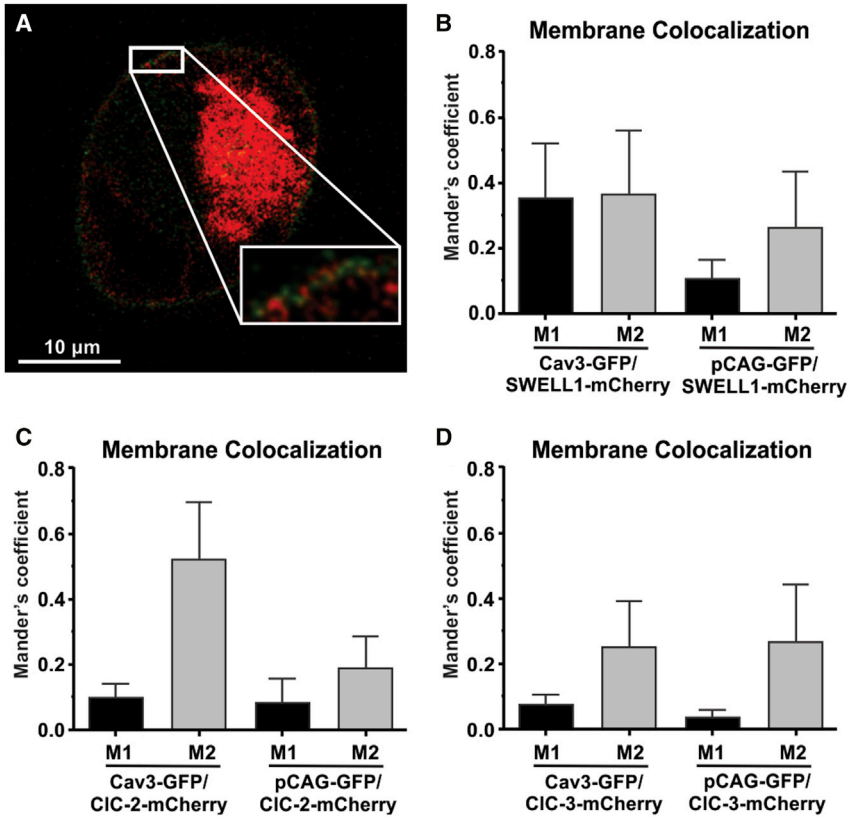

FIGURE 9 Membrane colocalization of Cav3-GFP, pCAG-GFP, SWELL1-mCherry, ClC-2-mCherry, and ClC-3 mCherry. (*A*) Representative image of Cav3-GFP and SWELL1-mCherry membrane colocalization. (*B-D*) Mander's coefficients of Cav3-GFP/SWELL1-mCherry and pCAG-GFP/SWELL1-mCherry (*B*), Cav3-GFP/ClC-2-mCHerry and pCAG-GFP/ClC-2-mCherry (*C*), and Cav3-GFP/ClC-mCherry and pCAG-GFP/ClC-3-mCherry (*D*).

type 1 receptors (65). Because Cav1 and Cav3 form hetero-oligomeric complexes in atrial cardiac myocytes (60), we suspect it may have a similar role with SWELL1, as indicated by the presence of an intracellular SWELL1/Cav3 FRET signal (Fig. 7). This interaction may be conducted by the caveolin scaffolding domain (which may interact with CBMs) and may be required for membrane localization. Given that this chaperone system may apply to SWELL1, the effect of lipid-mediated protein stabilization, and our qPCR findings, we speculate that caveolar lipid rafts may play a role in decreasing associated membrane protein turnover by increasing their stability, maintaining the normal demand for SWELL1 mRNA availability despite upregulated protein expression. Lowered FRET efficiency to pCAG-GFP control levels in response to hypotonic solution between Cav3 and SWELL1 indicates that their association is dependent on membrane mechanical tension. Although no FRET efficiency changes are observed inside the cell, the occurrence of intracellular FRET indicates that MCCs and Cav3 may traffic together to caveolar lipid rafts, which is common for other caveola-associated proteins (57,58). The lack of intracellular FRET efficiency change from isotonic to hypotonic is congruent with findings by König et al. which indicated that hypotonicity does not activate intracellular SWELL1 (58). We also found that caveola disruption via MβCD-induced cholesterol depletion reduced Cav3/SWELL1 interaction similar to that induced by hypotonic solution, suggesting that their interaction may also be dependent on caveola lipid raft integrity. Data from Kozera et al. (6) indicates that hypotonic and MβCD solutions reduce caveola density and induce $I_{Cl,swell}$ in rat ventricular cardiomyocytes. Lim et al. (66) found that MβCD and hypoosmotic-induced swelling activates $I_{Cl,swell}$ in human epithelial intestinal cells and skin fibroblasts but is blocked by cholesterol-loaded MβCD. Given these findings, it is likely that the association between Cav3 and SWELL1 is disrupted by caveola loss from increased membrane tension or cholesterol depletion and that loss of this interaction may be involved in activation of $I_{Cl,swell}$. This inhibitory effect of caveolin interaction is also observed with other proteins, such as nitric oxide synthases, thioredoxin reductase 1, T-type calcium channels, and potassium channels responsible for I_{to} (65,67–69). Given that Cav3/ClC-2/ClC-3 FRET efficiencies are unchanged by hypotonic stress and are less associated than pCAG-GFP controls, Cav3 is less likely to have a regulatory effect with these MCCs relative to SWELL1; therefore, Cav3 may not have this inhibitory effect on ClC-2 and ClC-3 activation in HEK293 cells and possibly myocytes.

Our cell swelling experiments recapitulate earlier findings (1,8,14) showing that Cav3 plays an important mechanoprotective role in buffering mechanical forces. More importantly, this protection is abolished by the presence of DCPIB, demonstrating that the mechanoprotective role of

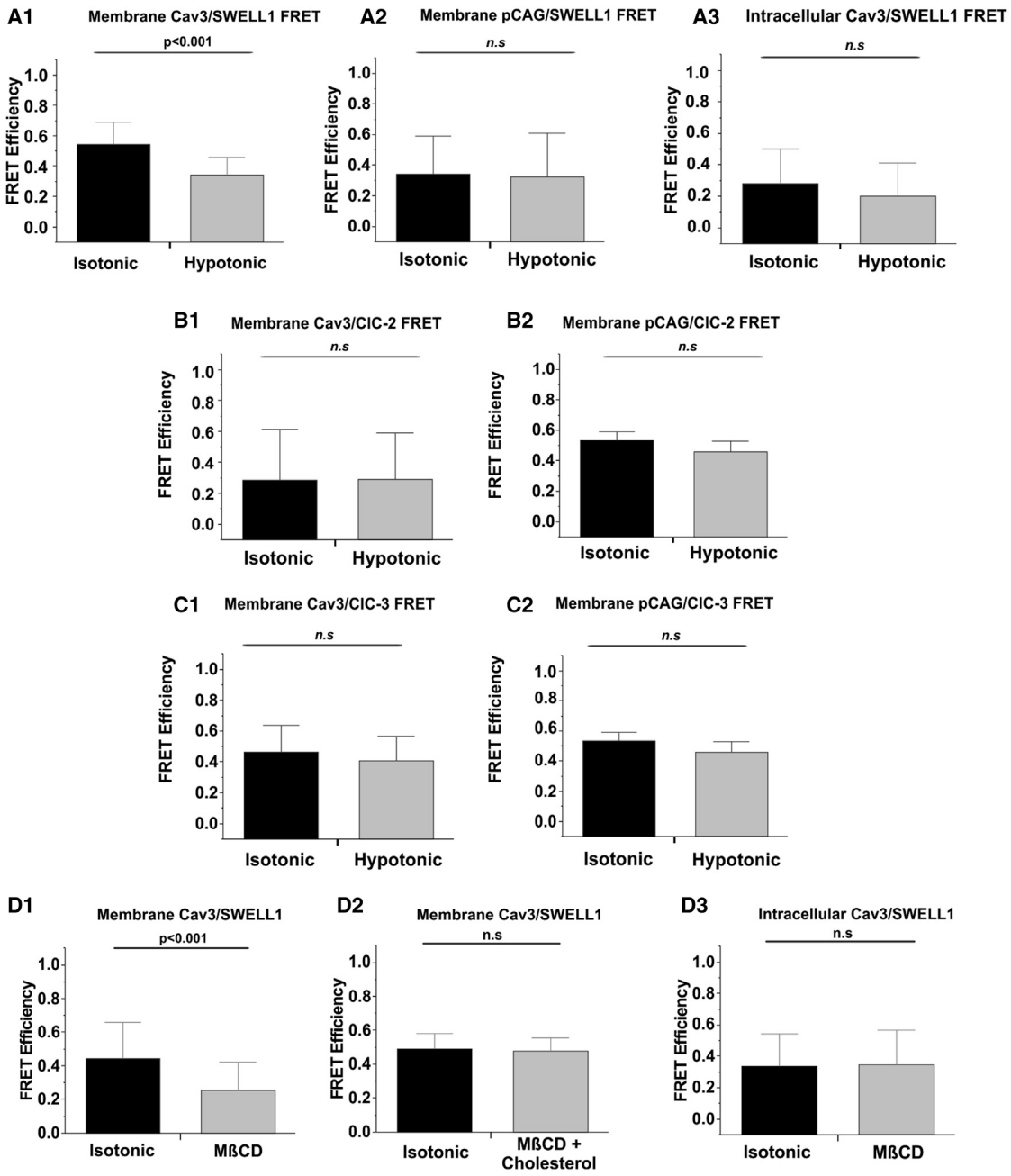

FIGURE 10 Cav3/MCC and pCAG/MCC FRET quantification under Iso (1 T), Hypo (0.7 T), and MβCD conditions. (A–C) Summarized FRET results for the membrane Cav3/MCC FRET (*A1*, *B1*, and *C1*), membrane control pCAG/SWELL1 (*A2*, *B2*, and *C2*), and intracellular Cav3/SWELL1 FRET (*A3*). FRET quantifications for baseline (Iso, 1 T) and after 1-h incubation with 10 mM MβCD Iso conditions, alone or together with 6.5 μM cholesterol for membrane Cav3/SWELL1 FRET (*D1*), cholesterol control Cav3/SWELL1 FRET (*D2*), and intracellular Cav3/SWELL1 FRET (*D3*). $N = 9$ cells/group, 10–15 FRET signals collected/cell, $N = 3$ transfections. Mean ± SD. p Values determined by paired Student's *t*-tests.

Cav3 is partially imparted by the enrichment of SWELL1 channels and their activity ($I_{Cl,swell}$) in HEK293 cells. These findings are also recapitulated in isolated mouse ventricular myocytes, where the percentage of membrane-damaged myocytes increases in DCPIB- and MβCD-treated cells. This is congruent with findings from Li et al. (25), who found that inhibition of various LRRC8 subunits (SWELL1 is also known as LRRC8A) increased hypotonically induced cell death in HeLa cells. Relevant to ischemia-induced cardiac hypoxia, Sforna et al. (24) showed that hypoxia induces $I_{Cl,swell}$ in glioblastoma multiforme cancer cells, in which caveolae have been shown to play a pro-survival role (70,71), and that application of DCPIB induced cell death. Souktani et al. (72) found that inhibition of swelling-activated chloride channels increased apoptosis and infarct size during ischemia-reperfusion injury in rabbit hearts. Our

data and those of others suggest a short-term pro-survival role of $I_{Cl,swell}$ activation, but this is contrasted by various studies that associate excess $I_{Cl,swell}$ with cell death (73,74) and indicate a still incomplete understanding of how MCCs contribute to cell survival.

These findings are relevant to cardiac health because constitutive $I_{Cl,swell}$ activity, accompanied by downregulation of caveolae and Cav3, has been implicated in various cardiac pathogeneses (1,38,39). We have also demonstrated that MCCs may contribute to stretch-induced arrhythmogenesis in the pulmonary veins (1), the main source of ectopic activity responsible for triggering atrial fibrillation in humans. This study demonstrates that Cav3 may specifically have an inhibitory effect on SWELL1 activity and that this effect may be abolished by membrane mechanical stress and disruption of caveola structures during chronic hypertension.

AUTHOR CONTRIBUTIONS

D.T. designed, performed, and analyzed data and was the principal writer of the manuscript for all experiments except for patch clamp-related work. L.T. designed, performed, and analyzed data and wrote all patch-clamp-related experiments. F.C.D. and R.Y.M. designed and performed cardiomyocyte swelling experiments. S.J.S. designed and performed qPCR experiments. D.L. designed and edited the manuscript. A.V.G. set experimental goals, aided with design of various experiments, and made major contributions to writing of the manuscript.

ACKNOWLEDGMENTS

This work was supported by NIH 1R01HL141214, AHA 16SDG29120011, and the University of Wisconsin Foundation Wisconsin Partnership Program grant 4140 (to A.V.G.). D.G.P.T. would like to acknowledge NIH predoctoral training grant T32GM008688, support provided by the University of Wisconsin-Madison Office of the Vice Chancellor for Research and Graduate Education with funding from the Wisconsin Alumni Research Foundation, and an AHA predoctoral fellowship (903203). We thank the AHA for supporting R.Y.M. via an AHA postdoctoral fellowship (915335) and University of WIsconsin-Madison for their support of F.C.D. via the Hilldale Undergraduate Research Fellowship. We also thank Drs. Timothy J. Kamp and Lee L. Eckhardt for crucial reagents for these experiments. Last, we thank Randall J. Massey and the SMPH Electron Microscopy Facility (University of Wisconsin-Madison) for critical assistance in preparing and imaging HEK293 cell caveolae.

REFERENCES

1. Egorov, Y. V., D. Lang, …, A. V. Glukhov. 2019. Caveolae-mediated activation of mechanosensitive chloride channels in pulmonary veins triggers atrial arrhythmogenesis. *J. Am. Heart Assoc.* 8:e012748. https://doi.org/10.1161/JAHA.119.012748. https://www.ncbi.nlm.nih.gov/pubmed/31597508.

2. Trouet, D., D. Hermans, …, J. Eggermont. 2001. Inhibition of volume-regulated anion channels by dominant-negative caveolin-1. *Biochem. Biophys. Res. Commun.* 284:461–465. https://doi.org/10.1006/bbrc.2001.4995. https://www.ncbi.nlm.nih.gov/pubmed/11394902.

3. Trouet, D., B. Nilius, …, J. Eggermont. 1999. Caveolin-1 modulates the activity of the volume-regulated chloride channel. *J. Physiol.* 520 Pt 1:113–119. http://www.ncbi.nlm.nih.gov/pubmed/10517805.

4. Eggermont, J., D. Trouet, …, B. Nilius. 2001. Cellular function and control of volume-regulated anion channels. *Cell Biochem Biophys.* 35:263–274. https://doi.org/10.1385/CBB:35:3:263. https://www.ncbi.nlm.nih.gov/pubmed/11894846.

5. Parton, R. G., and M. A. del Pozo. 2013. Caveolae as plasma membrane sensors, protectors and organizers. *Nat. Rev. Mol. Cell Biol.* 14:98–112. https://doi.org/10.1038/nrm3512. https://www.ncbi.nlm.nih.gov/pubmed/23340574.

6. Kozera, L., E. White, and S. Calaghan. 2009. Caveolae act as membrane reserves which limit mechanosensitive I(Cl,swell) channel activation during swelling in the rat ventricular myocyte. *PLoS One.* 4:e8312. https://doi.org/10.1371/journal.pone.0008312. http://www.ncbi.nlm.nih.gov/pubmed/20011535.

7. Pfeiffer, E. R., A. T. Wright, …, A. D. McCulloch. 2014. Caveolae in ventricular myocytes are required for stretch-dependent conduction slowing. *J. Mol. Cell Cardiol.* 76:265–274. https://doi.org/10.1016/j.yjmcc.2014.09.014. http://www.ncbi.nlm.nih.gov/pubmed/25257915.

8. Wei, E. Q., D. S. Sinden, …, G. S. Pitt. 2017. Inducible Fgf13 ablation enhances caveolae-mediated cardioprotection during cardiac pressure overload. *Proc. Natl. Acad. Sci. U S A.* 114:E4010–E4019. https://doi.org/10.1073/pnas.1616393114. http://www.ncbi.nlm.nih.gov/pubmed/28461495.

9. Gabella, G. 1978. Inpocketings of the cell membrane (caveolae) in the rat myocardium. *J. Ultrastruct. Res.* 65:135–147 (Comparative Study). http://www.ncbi.nlm.nih.gov/pubmed/731782.

10. Masson-Pevet, M., D. Gros, and E. Besselsen. 1980. The caveolae in rabbit sinus node and atrium. *Cell Tissue Res.* 208:183–196. http://www.ncbi.nlm.nih.gov/pubmed/7407830.

11. Parton, R. G., and K. Simons. 2007. The multiple faces of caveolae. *Nat. Rev. Mol. Cell Biol.* 8:185–194. https://doi.org/10.1038/nrm2122. http://www.ncbi.nlm.nih.gov/pubmed/17318224.

12. Sinha, B., D. Koster, …, P. Nassoy. 2011. Cells respond to mechanical stress by rapid disassembly of caveolae. *Cell.* 144:402–413. https://doi.org/10.1016/j.cell.2010.12.031. http://www.ncbi.nlm.nih.gov/pubmed/21295700.

13. Torrino, S., W. W. Shen, …, C. Lamaze. 2018. EHD2 is a mechanotransducer connecting caveolae dynamics with gene transcription. *J. Cell Biol.* 217:4092–4105. https://doi.org/10.1083/jcb.201801122. https://www.ncbi.nlm.nih.gov/pubmed/30348749.

14. Sun, J., T. Nguyen, …, E. Murphy. 2013. Cardioprotective role of caveolae in ischemia-reperfusion injury. *Transl Med. (Sunnyvale).* 3:1000114. https://doi.org/10.4172/2161-1025.1000114. https://www.ncbi.nlm.nih.gov/pubmed/26989575.

15. Baumgarten, C. M., and H. F. Clemo. 2003. Swelling-activated chloride channels in cardiac physiology and pathophysiology. *Prog. Biophys. Mol. Biol.* 82:25–42. https://doi.org/10.1016/s0079-6107(03)00003-8. https://www.ncbi.nlm.nih.gov/pubmed/12732266.

16. Huang, Z. M., C. Prasad, …, D. Duan. 2009. Functional role of CLC-2 chloride inward rectifier channels in cardiac sinoatrial nodal pacemaker cells. *J. Mol. Cell Cardiol.* 47:121–132. https://doi.org/10.1016/j.yjmcc.2009.04.008. http://www.ncbi.nlm.nih.gov/pubmed/19376127.

17. Couet, J., S. Li, …, M. P. Lisanti. 1997. Identification of peptide and protein ligands for the caveolin-scaffolding domain. Implications for the interaction of caveolin with caveolae-associated proteins. *J. Biol. Chem.* 272:6525–6533. https://doi.org/10.1074/jbc.272.10.6525. https://www.ncbi.nlm.nih.gov/pubmed/9045678.

18. Rothberg, K. G., J. E. Heuser, …, R. G. Anderson. 1992. Caveolin, a protein component of caveolae membrane coats. *Cell.* 68:673–682. http://www.ncbi.nlm.nih.gov/pubmed/1739974.

19. Smart, E. J., G. A. Graf, …, M. P. Lisanti. 1999. Caveolins, liquid-ordered domains, and signal transduction. *Mol. Cell Biol.* 19:7289–7304. https://doi.org/10.1128/MCB.19.11.7289. https://www.ncbi.nlm.nih.gov/pubmed/10523618.

20. Collins, B. M., M. J. Davis, …, R. G. Parton. 2012. Structure-based reassessment of the caveolin signaling model: do caveolae regulate signaling through caveolin-protein interactions? *Dev. Cell.* 23:11–20.

https://doi.org/10.1016/j.devcel.2012.06.012. https://www.ncbi.nlm.nih.gov/pubmed/22814599.

21. Helix, N., D. Strobaek, …, P. Christophersen. 2003. Inhibition of the endogenous volume-regulated anion channel (VRAC) in HEK293 cells by acidic di-aryl-ureas. *J. Membr. Biol.* 196:83–94. https://doi.org/10.1007/s00232-003-0627-x. https://www.ncbi.nlm.nih.gov/pubmed/14724745.

22. Chubinskiy-Nadezhdin, V. I., Y. A. Negulyaev, and E. A. Morachevskaya. 2011. Cholesterol depletion-induced inhibition of stretch-activated channels is mediated via actin rearrangement. *Biochem. biophysical Res. Commun.* 412:80–85. https://doi.org/10.1016/j.bbrc.2011.07.046. https://www.ncbi.nlm.nih.gov/pubmed/21798240.

23. Raucci, F. J., Jr., D. S. Wijesinghe, …, C. M. Baumgarten. 2010. Exogenous and endogenous ceramides elicit volume-sensitive chloride current in ventricular myocytes. *Cardiovasc. Res.* 86:55–62. https://doi.org/10.1093/cvr/cvp399. https://www.ncbi.nlm.nih.gov/pubmed/20008476.

24. Sforna, L., M. Cenciarini, …, L. Catacuzzeno. 2017. Hypoxia modulates the swelling-activated Cl current in human glioblastoma cells: role in volume regulation and cell survival. *J. Cell Physiol.* 232:91–100. https://doi.org/10.1002/jcp.25393. https://www.ncbi.nlm.nih.gov/pubmed/27028592.

25. Li, P., M. Hu, …, H. Xu. 2020. LRRC8 family proteins within lysosomes regulate cellular osmoregulation and enhance cell survival to multiple physiological stresses. *Proc. Natl. Acad. Sci. U S A.* 117:29155–29165. https://doi.org/10.1073/pnas.2016539117. https://www.ncbi.nlm.nih.gov/pubmed/33139539.

26. Peyronnet, R., J. M. Nerbonne, and P. Kohl. 2016. Cardiac mechano-gated ion channels and arrhythmias. *Circ. Res.* 118:311–329. https://doi.org/10.1161/CIRCRESAHA.115.305043. http://www.ncbi.nlm.nih.gov/pubmed/26838316.

27. Turner, D., C. Kang, …, R. Sah. 2021. Electrophysiological and molecular mechanisms of sinoatrial node Mechanosensitivity. *Front. Cardiovasc. Med.* 8:662410. https://doi.org/10.3389/fcvm.2021.662410. https://www.ncbi.nlm.nih.gov/pubmed/34434970.

28. Kelly, D., L. Mackenzie, …, D. A. Saint. 2006. Gene expression of stretch-activated channels and mechanoelectric feedback in the heart. *Clin. Exp. Pharmacol. Physiol.* 33:642–648. https://doi.org/10.1111/j.1440-1681.2006.04392.x. https://www.ncbi.nlm.nih.gov/pubmed/16789934.

29. Xian Tao, L., V. Dyachenko, …, J. Daut. 2006. The stretch-activated potassium channel TREK-1 in rat cardiac ventricular muscle. *Cardiovasc. Res.* 69:86–97. https://doi.org/10.1016/j.cardiores.2005.08.018. https://www.ncbi.nlm.nih.gov/pubmed/16248991.

30. Noel, J., G. Sandoz, and F. Lesage. 2011. Molecular regulations governing TREK and TRAAK channel functions. *Channels (Austin).* 5:402–409. https://doi.org/10.4161/chan.5.5.16469. https://www.ncbi.nlm.nih.gov/pubmed/21829087.

31. Takahashi, K., and K. Naruse. 2012. Stretch-activated BK channel and heart function. *Prog. Biophys. Mol. Biol.* 110:239–244. https://doi.org/10.1016/j.pbiomolbio.2012.08.001. https://www.ncbi.nlm.nih.gov/pubmed/23281538.

32. Dyachenko, V., B. Husse, …, G. Isenberg. 2009. Mechanical deformation of ventricular myocytes modulates both TRPC6 and Kir2.3 channels. *Cell Calcium.* 45:38–54. https://doi.org/10.1016/j.ceca.2008.06.003. https://www.ncbi.nlm.nih.gov/pubmed/18635261.

33. Pedrozo, Z., A. Criollo, …, J. A. Hill. 2015. Polycystin-1 is a cardiomyocyte mechanosensor that Governs L-type Ca2+ channel protein stability. *Circulation.* 131:2131–2142. https://doi.org/10.1161/CIRCULATIONAHA.114.013537. https://www.ncbi.nlm.nih.gov/pubmed/25888683.

34. Boycott, H. E., C. S. Barbier, …, E. Balse. 2013. Shear stress triggers insertion of voltage-gated potassium channels from intracellular compartments in atrial myocytes. *Proc. Natl. Acad. Sci. U S A.* 110:E3955–E3964. https://doi.org/10.1073/pnas.1309896110. https://www.ncbi.nlm.nih.gov/pubmed/24065831.

35. Quinn, T. A., and P. Kohl. 2021. Cardiac mechano-electric coupling: acute effects of mechanical stimulation on heart rate and rhythm. *Physiol. Rev.* 101:37–92. https://doi.org/10.1152/physrev.00036.2019. https://www.ncbi.nlm.nih.gov/pubmed/32380895.

36. Fedorov, V. V., O. P. Trifonova, …, L. V. Rosenshtraukh. 2005. The role of mechano-electrical feedback in the cholinergic atrial fibrillation initiation. *In* Mechanosensitivity in Cells and Tissue. A. Kamkin and I. Kiseleva, eds Academia, Moscow, pp. 313–335.

37. Arai, A., I. Kodama, and J. Toyama. 1996. Roles of Cl- channels and Ca2+ mobilization in stretch-induced increase of SA node pacemaker activity. *Am. J. Physiol.* 270:H1726–H1735. https://doi.org/10.1152/ajpheart.1996.270.5.H1726. https://www.ncbi.nlm.nih.gov/pubmed/8928880.

38. Shi, H., Z. Jiang, …, F. Cao. 2019. Elevated swelling-activated chloride current densities in hypertrophied ventricular myocytes in a rabbit heart failure model. *Heart Surg. Forum.* 22:E107–E111. https://doi.org/10.1532/hsf.2255. https://www.ncbi.nlm.nih.gov/pubmed/31013219.

39. Clemo, H. F., B. S. Stambler, and C. M. Baumgarten. 1999. Swelling-activated chloride current is persistently activated in ventricular myocytes from dogs with tachycardia-induced congestive heart failure. *Circ. Res.* 84:157–165. http://www.ncbi.nlm.nih.gov/pubmed/9933247.

40. Wong, R., A. Abussaud, …, H. S. Sun. 2018. Blockade of the swelling-induced chloride current attenuates the mouse neonatal hypoxic-ischemic brain injury in vivo. *Acta Pharmacol. Sin.* 39:858–865. https://doi.org/10.1038/aps.2018.1. https://www.ncbi.nlm.nih.gov/pubmed/29595192.

41. Greenwood, I. A. 2004. CLC-3 knockout hints at swelling-activated chloride channel complexity. *J. Physiol.* 557:343. https://doi.org/10.1113/jphysiol.2004.063750. https://www.ncbi.nlm.nih.gov/pubmed/15020689.

42. Qiu, Z., A. E. Dubin, …, A. Patapoutian. 2014. SWELL1, a plasma membrane protein, is an essential component of volume-regulated anion channel. *Cell.* 157:447–458. https://doi.org/10.1016/j.cell.2014.03.024. https://www.ncbi.nlm.nih.gov/pubmed/24725410.

43. Voss, F. K., F. Ullrich, …, T. J. Jentsch. 2014. Identification of LRRC8 heteromers as an essential component of the volume-regulated anion channel VRAC. *Science.* 344:634–638. https://doi.org/10.1126/science.1252826. https://www.ncbi.nlm.nih.gov/pubmed/24790029.

44. Soliman, C., S. Eastwood, …, A. Elbourne. 2019. The membrane effects of melittin on gastric and colorectal cancer. *PLoS One.* 14:e0224028. https://doi.org/10.1371/journal.pone.0224028. https://www.ncbi.nlm.nih.gov/pubmed/31622415.

45. Tan, J. M. J., N. Mellouk, …, J. H. Brumell. 2018. An ATG16L1-dependent pathway promotes plasma membrane repair and limits Listeria monocytogenes cell-to-cell spread. *Nat. Microbiol.* 3:1472–1485. https://doi.org/10.1038/s41564-018-0293-5. https://www.ncbi.nlm.nih.gov/pubmed/30478389.

46. Babiychuk, E. B., K. Monastyrskaya, …, A. Draeger. 2011. Blebbing confers resistance against cell lysis. *Cell Death Differ.* 18:80–89. https://doi.org/10.1038/cdd.2010.81. https://www.ncbi.nlm.nih.gov/pubmed/20596076.

47. Reilly, L., F. J. Alvarado, …, L. L. Eckhardt. 2020. Genetic loss of Ik1 causes adrenergic-induced phase 3 early afterdepolarizations and polymorphic and bidirectional ventricular tachycardia. *Circ. Arrhythm Electrophysiol.* 13:e008638. https://doi.org/10.1161/CIRCEP.120.008638. https://www.ncbi.nlm.nih.gov/pubmed/32931337.

48. Lang, D., R. Y. Medvedev, …, A. V. Glukhov. 2022. Region-specific distribution of transversal-axial tubule system organization underlies heterogeneity of calcium dynamics in the right atrium. *Am. J. Physiol. Heart Circ. Physiol.* 322:H269–H284. https://doi.org/10.1152/ajpheart.00381.2021. https://www.ncbi.nlm.nih.gov/pubmed/34951544.

49. van Rheenen, J., M. Langeslag, and K. Jalink. 2004. Correcting confocal acquisition to optimize imaging of fluorescence resonance energy transfer by sensitized emission. *Biophys. J.* 86:2517–2529. https://doi.org/10.1016/S0006-3495(04)74307-6. https://www.ncbi.nlm.nih.gov/pubmed/15041688.

50. Li, H., W. Yao, …, Z. Xia. 2016. Hyperglycemia abrogates ischemic postconditioning cardioprotection by impairing

AdipoR1/caveolin-3/STAT3 signaling in diabetic rats. *Diabetes.* 65:942–955. https://doi.org/10.2337/db15-0782. https://www.ncbi.nlm.nih.gov/pubmed/26718505.

51. Yang, Y., Z. Ma, …, W. Yi. 2016. Caveolin-1/-3: therapeutic targets for myocardial ischemia/reperfusion injury. *Basic Res. Cardiol.* 111:45. https://doi.org/10.1007/s00395-016-0561-6. https://www.ncbi.nlm.nih.gov/pubmed/27282376.
52. See Hoe, L. E., J. M. Schilling, …, J. N. Peart. 2014. Sarcolemmal cholesterol and caveolin-3 dependence of cardiac function, ischemic tolerance, and opioidergic cardioprotection. *Am. J. Physiol. Heart Circ. Physiol.* 307:H895–H903. https://doi.org/10.1152/ajpheart.00081.2014. https://www.ncbi.nlm.nih.gov/pubmed/25063791.
53. Yallop, C. A., and I. Svendsen. 2001. The effects of G418 on the growth and metabolism of recombinant mammalian cell lines. *Cytotechnology.* 35:101–114. https://doi.org/10.1023/A:1017550902771. https://www.ncbi.nlm.nih.gov/pubmed/19003287.
54. Lv, J., Y. Liang, …, P. Zhou. 2019. DCPIB, an inhibitor of volume-regulated anion channels, distinctly modulates K2P channels. *ACS Chem. Neurosci.* 10:2786–2793. https://doi.org/10.1021/acschemneuro.9b00010. https://www.ncbi.nlm.nih.gov/pubmed/30935201.
55. Balijepalli, R. C., B. P. Delisle, …, C. T. January. 2007. Kv11.1 (ERG1) K+ channels localize in cholesterol and sphingolipid enriched membranes and are modulated by membrane cholesterol. *Channels (Austin).* 1:263–272. http://www.ncbi.nlm.nih.gov/pubmed/18708743.
56. Vaidyanathan, R., A. L. Vega, …, L. L. Eckhardt. 2013. The interaction of caveolin 3 protein with the potassium inward rectifier channel Kir2.1: physiology and pathology related to long qt syndrome 9 (LQT9). *J. Biol. Chem.* 288:17472–17480. https://doi.org/10.1074/jbc.M112.435370. http://www.ncbi.nlm.nih.gov/pubmed/23640888.
57. Suzuki, Y., H. Yamamura, …, Y. Imaizumi. 2013. Direct molecular interaction of caveolin-3 with KCa1.1 channel in living HEK293 cell expression system. *Biochem. biophysical Res. Commun.* 430:1169–1174. https://doi.org/10.1016/j.bbrc.2012.12.015. https://www.ncbi.nlm.nih.gov/pubmed/23237801.
58. Konig, B., Y. Hao, …, T. Stauber. 2019. A FRET sensor of C-terminal movement reveals VRAC activation by plasma membrane DAG signaling rather than ionic strength. *Elife.* 8:e45421. https://doi.org/10.7554/eLife.45421. https://www.ncbi.nlm.nih.gov/pubmed/31210638.
59. Byrne, D. P., C. Dart, and D. J. Rigden. 2012. Evaluating caveolin interactions: do proteins interact with the caveolin scaffolding domain through a widespread aromatic residue-rich motif? *PLoS One.* 7:e44879. https://doi.org/10.1371/journal.pone.0044879. https://www.ncbi.nlm.nih.gov/pubmed/23028656.
60. Volonte, D., C. F. McTiernan, …, F. Galbiati. 2008. Caveolin-1 and caveolin-3 form heterooligomeric complexes in atrial cardiac myocytes that are required for doxorubicin-induced apoptosis. *Am. J. Physiol. Heart Circ. Physiol.* 294:H392–H401. https://doi.org/10.1152/ajpheart.01039.2007. https://www.ncbi.nlm.nih.gov/pubmed/17982011.
61. Koussounadis, A., S. P. Langdon, …, V. A. Smith. 2015. Relationship between differentially expressed mRNA and mRNA-protein correlations in a xenograft model system. *Scientific Rep.* 5:10775. https://doi.org/10.1038/srep10775. https://www.ncbi.nlm.nih.gov/pubmed/26053859.
62. Seddon, A. M., P. Curnow, and P. J. Booth. 2004. Membrane proteins, lipids and detergents: not just a soap opera. *Biochim. Biophys. Acta.* 1666:105–117. https://doi.org/10.1016/j.bbamem.2004.04.011. https://www.ncbi.nlm.nih.gov/pubmed/15519311.
63. Nji, E., Y. Chatzikyriakidou, …, D. Drew. 2018. An engineered thermal-shift screen reveals specific lipid preferences of eukaryotic and prokaryotic membrane proteins. *Nat. Commun.* 9:4253. https://doi.org/10.1038/s41467-018-06702-3. https://www.ncbi.nlm.nih.gov/pubmed/30315156.
64. Wyse, B. D., I. A. Prior, …, J. F. Hancock. 2003. Caveolin interacts with the angiotensin II type 1 receptor during exocytic transport but not at the plasma membrane. *J. Biol. Chem.* 278:23738–23746. https://doi.org/10.1074/jbc.M212892200. https://www.ncbi.nlm.nih.gov/pubmed/12692121.
65. Tyan, L., D. Turner, …, A. V. Glukhov. 2021. Caveolin-3 is required for regulation of transient outward potassium current by angiotensin II in mouse atrial myocytes. *Am. J. Physiol. Heart Circ. Physiol.* 320:H787–H797. https://doi.org/10.1152/ajpheart.00569.2020. https://www.ncbi.nlm.nih.gov/pubmed/33416459.
66. Lim, C. H., K. Schoonderwoerd, …, B. C. Tilly. 2006. Regulation of the cell swelling-activated chloride conductance by cholesterol-rich membrane domains. *Acta Physiol. (Oxf).* 187:295–303. https://doi.org/10.1111/j.1748-1716.2006.01534.x. https://www.ncbi.nlm.nih.gov/pubmed/16734766.
67. Venema, V. J., H. Ju, …, R. C. Venema. 1997. Interaction of neuronal nitric-oxide synthase with caveolin-3 in skeletal muscle. Identification of a novel caveolin scaffolding/inhibitory domain. *J. Biol. Chem.* 272:28187–28190. https://doi.org/10.1074/jbc.272.45.28187. https://www.ncbi.nlm.nih.gov/pubmed/9353265.
68. Volonte, D., and F. Galbiati. 2009. Inhibition of thioredoxin reductase 1 by caveolin 1 promotes stress-induced premature senescence. *EMBO Rep.* 10:1334–1340. https://doi.org/10.1038/embor.2009.215. https://www.ncbi.nlm.nih.gov/pubmed/19820694.
69. Markandeya, Y. S., L. J. Phelan, …, R. C. Balijepalli. 2015. Caveolin-3 overexpression attenuates cardiac hypertrophy via inhibition of T-type Ca2+ current modulated by protein kinase calpha in cardiomyocytes. *J. Biol. Chem.* 290:22085–22100. https://doi.org/10.1074/jbc.M115.674945. http://www.ncbi.nlm.nih.gov/pubmed/26170457.
70. Hehlgans, S., and N. Cordes. 2011. Caveolin-1: an essential modulator of cancer cell radio-and chemoresistance. *Am. J. Cancer Res.* 1:521–530. https://www.ncbi.nlm.nih.gov/pubmed/21984970.
71. Yamaguchi, T., C. Lu, …, T. Takahashi. 2016. ROR1 sustains caveolae and survival signalling as a scaffold of cavin-1 and caveolin-1. *Nat. Commun.* 7:10060. https://doi.org/10.1038/ncomms10060. https://www.ncbi.nlm.nih.gov/pubmed/26725982.
72. Souktani, R., B. Ghaleb, …, A. Berdeaux. 2003. Inhibitors of swelling-activated chloride channels increase infarct size and apoptosis in rabbit myocardium. *Fundam. Clin. Pharmacol.* 17:555–561. https://doi.org/10.1046/j.1472-8206.2003.00175.x. https://www.ncbi.nlm.nih.gov/pubmed/14703716.
73. Xia, Y., Y. Liu, …, X. Wang. 2016. Activation of volume-sensitive Cl- channel mediates autophagy-related cell death in myocardial ischaemia/reperfusion injury. *Oncotarget.* 7:39345–39362. https://doi.org/10.18632/oncotarget.10050. https://www.ncbi.nlm.nih.gov/pubmed/27322431.
74. Zhou, J. J., Y. Luo, …, H. L. Pan. 2020. LRRC8A-dependent volume-regulated anion channels contribute to ischemia-induced brain injury and glutamatergic input to hippocampal neurons. *Exp. Neurol.* 332:113391. https://doi.org/10.1016/j.expneurol.2020.113391. https://www.ncbi.nlm.nih.gov/pubmed/32598930.
75. Busija, A. R., H. H. Patel, and P. A. Insel. 2017. Caveolins and cavins in the trafficking, maturation, and degradation of caveolae: implications for cell physiology. *Am. J. Physiol. Cell Physiol.* 312:C459–C477. https://doi.org/10.1152/ajpcell.00355.2016. https://www.ncbi.nlm.nih.gov/pubmed/28122734.